Inorganic Chemistry

pubs.acs.org/IC Article

Half-Sandwich Ru(*p*-cymene) Compounds with Diphosphanes: *In Vitro* and *In Vivo* Evaluation As Potential Anticancer Metallodrugs

Oscar A. Lenis-Rojas, M. Paula Robalo, Ana Isabel Tomaz,* Alexandra R. Fernandes,* Catarina Roma-Rodrigues, Ricardo G. Teixeira, Fernanda Marques, Mónica Folgueira, Julián Yáñez, Anabel Alba Gonzalez, Martín Salamini-Montemurri, Dawrin Pech-Puch, Digna Vázquez-García, Margarita López Torres, Alberto Fernández, and Jesús J. Fernández*

Cite This: *Inorg. Chem.* 2021, 60, 2914–2930 Read Online

ACCESS | Metrics & More | Article Recommendations | Supporting Information

ABSTRACT: Ruthenium(II) complexes are currently considered attractive alternatives to the widely used platinum-based drugs. We present herein the synthesis and characterization of half-sandwich ruthenium compounds formulated as [Ru(*p*-cymene)(L)Cl]-[CF_3SO_3] (L = 1,1-bis(methylenediphenylphosphano)ethylene, **1**; L = 1,1-bis(diphenylphosphano)ethylene, **2**), which were characterized by elemental analysis, mass spectrometry, ^{1}H and ^{31}P{^{1}H} NMR, UV−vis and IR spectroscopy, conductivity measurements and cyclic voltammetry. The molecular structures for both complexes were determined by single-crystal X-ray diffraction. Their cytotoxic activity was evaluated using the MTT assay against human tumor cells, namely ovarian (A2780) and breast (MCF7 and MDA-MB-231). Both complexes were active against breast adenocarcinoma cells, with complex **1** exhibiting a quite remarkable cytotoxicity in the submicromolar range. Interestingly, at concentrations equivalent to the IC_{50} values in the MCF7 cancer cells, complexes **1** and **2** presented lower cytotoxicity in normal human primary fibroblasts. The antiproliferative effects of **1** and **2** in MCF7 cells might be associated with the induction of reactive oxygen species (ROS), leading to a combined cell death mechanism via apoptosis and autophagy. Despite the fact that *in vitro* a partial intercalation between complexes and DNA was observed, no MCF7 cell cycle delay or arrest was observed, indicating that DNA might not be a direct target. Complexes **1** and **2** both exhibited a moderate to strong interaction with human serum albumin, suggesting that protein targets may be involved in their mode of action. Their acute toxicity was evaluated in the zebrafish model. Complex **1** (the most toxic of the two) exhibited a lethal toxicity LC_{50} value about 1 order of magnitude higher than any IC_{50} concentrations found for the cancer cell models used, highlighting its therapeutic relevance as a drug candidate in cancer chemotherapy.

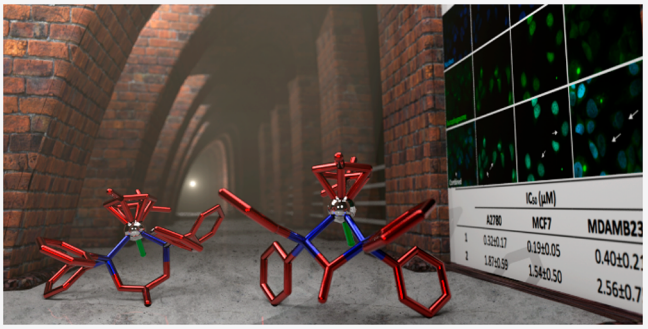

INTRODUCTION

Research in the field of cancer metallodrugs able to overcome the limitations of platinum-based chemotherapy,[1] currently used in clinical treatments, still represents one of the most important objectives in the field of applied inorganic chemistry.[2] Ruthenium compounds are regarded as promising candidates for the next generation of metal anticancer drugs, due to their low systemic toxicity and selective antimetastatic properties.[3] NAMI-A (imidazolium trans-[tetrachlorido(1*H*-imidazole)(*S*-dimethyl sulfoxide)ruthenate(III)]) and KP1019 (indazolium *trans*-[tetrachloridobis(1*H*-indazole)ruthenate-(III)]) and its more water-soluble sodium salt NKP1339, have been extensively studied, and in the case of NKP1339 (or IT-139), it is still in clinical trials.[4,5] Recently, the Ru(II) complex TLD1433 specifically designed for photodynamic therapy entered clinical trials (and is now in phase Ib)[6,7] (Figure 1).

Ruthenium(II) coordination compounds have been extensively studied over the last years, especially those derived from bipyridine and related ligands,[8,9] as well as organometallic ruthenium(II) compounds,[10,11] mainly derived from polyhapto ligands. The latter have attracted significant attention as anticancer candidates, in particular complexes based on the ruthenium(II) η^6-arene moiety[12] such as the RAPTA derivatives, bearing a 1,3,5-triaza-7-phosphatricyclo[3.3.1.1]-decane (PTA) ligand,[13] and RAED complexes, possessing ethylene-1,2-diamine (en) or related N,N ligands,[14] which are

Received: September 16, 2020
Published: February 11, 2021

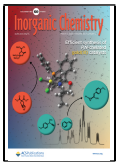

https://dx.doi.org/10.1021/acs.inorgchem.0c02768
Inorg. Chem. 2021, 60, 2914–2930

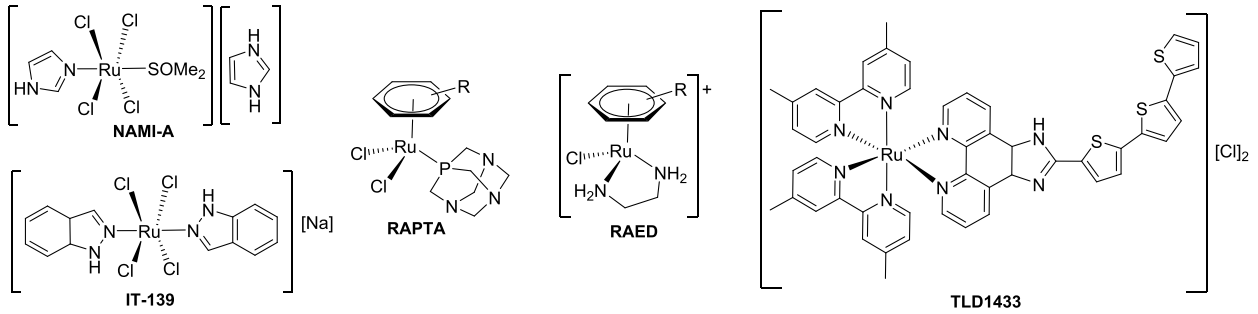

Figure 1. Relevant ruthenium compounds with anticancer activity.

considered to be prominent species with significant antitumor activity *in vivo* (Figure 1). Their mechanism of action depends on the arene moiety, on the bound coligand(s),[15] and even on the attached halide(s).[16] The halide(s) can undergo aquation under physiological conditions, allowing improved interactions with the biological target.[17−19] However, rapid aquation could lead to a percentage of the drug being inactive before it even reaches the target site.[20] The incorporation of less labile ligands such as phosphines enables a slower aquation process, while still maintaining cytotoxic activity.[21,22] A variety of complexes obtained by formal replacement of PTA with an alternative P ligand such as aminomethylphosphines,[23] aminophosphines,[24] triphenylphosphine,[25,26] and *o*-oxytriphenylphosphine[27] have been prepared and evaluated as anticancer agents, showing in general an activity comparable to that of cisplatin. Consequently, the half-sandwich ruthenium compounds with phosphine ligands represent a versatile and potential class of anticancer metallodrugs. For that, chemical development and biological studies of these systems could be fundamental for fighting cancer. Nevertheless, examples with P,P donor atoms are still scarce.[28]

Here we report the synthesis, characterization, electrochemical properties, and biological activity of two Ru(II) arene complexes derived from the Ru(*p*-cymene) fragment. The properties of these types of compounds depend on the nature of the ancillary ligands as well as of the metallic fragment; thus, we decided to evaluate the influence in the biological activity of bidentate ligands which could stabilize the Ru(arene) moiety, such as coordinated *P,P*-diphosphanes, with a σ-donor and π-acceptor character, which are scarce in the literature. The cellular internalization, cytotoxicity, cell death mechanism, cytostatic potential, and interaction with DNA molecules were also analyzed for these new complexes.

Bioavailability is of crucial importance when potential drug candidates are screened. Binding to plasma, proteins can exert a significant effect on drug distribution, pharmacokinetics, and bioavailability.[29,30] Human serum albumin (HSA) is the most abundant high-molecular-weight blood plasma constituent, with an extraordinary ability to bind both endogenous metabolic compounds and exogenous therapeutic drugs.[31] It exerts a significant effect on the drug performance *in vivo* since it can increase, slow down, or prevent passive extravasation into tissues.[29,30,32] Understanding the binding of these new complexes to HSA is thus a first approach to outline their pharmacokinetics.[30,33] In addition, HSA binding can be used to access more efficient tumor-selective drug delivery through passive targeting, given its accumulation in malignant and inflamed tissue.[32,34]

An *in vivo* toxicity evaluation of these *P,P*-diphosphane Ru complexes was developed on zebrafish embryos. We[9,35] and others[36] have previously used zebrafish embryos as a model for *in vivo* tests of other ruthenium complexes. Since its introduction in research in the 1990s, the zebrafish has proven to be an excellent animal model, nowadays being used for multiple purposes including toxicology and drug discovery,[37,38] and Environmental Agencies within the EU accept the OECD zebrafish test to assess water quality.[39] Here we have used the fish embryo acute toxicity (FET)[32] in order to test the lethal toxicity (LC_{50}) of compounds **1** and **2**.

EXPERIMENTAL SECTION

Materials and Methods. Solvents were reagent grade and were purified by standard methods.[40] Chemicals were purchased from Alfa Aesar and Sigma-Aldrich and used without further purification. Dichloro(*p*-cymene)ruthenium(II) dimer (97%, Sigma-Aldrich) was used as the ruthenium starting material for the complexes synthesized. HPLC separations were performed on an Agilent 1100 liquid chromatography system equipped with a solvent degasser, a quaternary pump, and a diode array detector (Agilent Technologies, Waldbronn, Germany) using a semipreparative reversed-phase column C18-Gemini 5 μm, 110 Å (250 × 10 mm). Microanalyses were carried out using a Carlo Erba Elemental Analyzer, Model 1108. IR spectra were recorded as Nujol mulls, polythene disks Nujol mulls, or KBr disks on a Satellite FTIR instrument. UV−vis spectra were collected on a Jasco V650 spectrophotometer. NMR spectra were obtained as DMSO-d_6 and CD_2Cl_2 solutions and referenced to $SiMe_4$ (^1H) or 85% H_3PO_4 ($^{31}P\{^1H\}$) and were recorded on Bruker Advance 300 spectrometers. All chemical shifts were reported downfield from standards. The FAB mass spectra were recorded using a FISONS Quatro mass spectrometer with a Cs ion gun; 3-nitrobenzyl alcohol was used as the matrix. Conductivity measurements were carried out on a CRISON GLP 32 conductivimeter using 10^{-3} mol dm^{-3} solutions in ethanol or acetone.

Synthetic Procedures. *Preparation of [Ru{p-C$_6$H$_4$(Me)(^{i}Pr)}{(Ph$_2$PCH$_2$)$_2$C=CH$_2$-P,P}Cl][CF$_3$SO$_3$] (**1**).* $AgCF_3SO_3$ (0.168 g, 0.654 mmol) was added to a solution of $[Ru(p\text{-cymene})(Cl)(\mu\text{-}Cl)]_2$ (0.200 g, 0.326 mmol) in 40 cm^3 of dichloromethane, and the mixture was stirred for 1 h at room temperature under argon. 1,1-Bis-(methylenediphenylphosphano)ethylene (0.276 g, 0.652 mmol) was added, and the mixture was stirred for 15 h at room temperature under an inert atmosphere. The resulting solution was filtered twice through Celite to remove the silver chloride that formed, and the solvent was removed under vacuum to give a yellow solid which was recrystallized from dichloromethane/*n*-hexane and was further purified by RP-HPLC with a mobile phase consisting of an isocratic at 100% CH_3OH at a flow rate of 2.0 mL/min to give **1** (t_R = 1.9 min).

Yield: 83%. Anal. Found: C, 55.1; H, 4.4. Calcd for $C_{39}H_{40}ClF_3O_3P_2RuS$: C, 55.5; H, 4.8. IR ($\nu_{max}/cm^{-1}$): 1261s [$\nu_{as}(SO_3)$], 1224sh [$\nu_s(CF_3)$], 1147s [$\nu_{as}(CF_3)$], 1030s [$\nu_s(SO_3)$]. UV−vis [EtOH, λ_{max}, nm (ε, M^{-1} cm^{-1})]: 416 (469), 325 (1948), 202 (26358). ^1H NMR (300 MHz, CD_2Cl_2, δ ppm, J in Hz): δ 7.76 [m, 4H, $H_{Ph\text{-}phosphane}$], 7.60 [m, 8H, $H_{Ph\text{-}phosphane}$], 7.5 [m, 4H, $H_{Ph\text{-}phosphane}$], 7.38 [m, 4H, $H_{Ph\text{-}phosphane}$], 5.88 [d, 2H, J(HH) = 8.4,

https://dx.doi.org/10.1021/acs.inorgchem.0c02768
Inorg. Chem. 2021, 60, 2914−2930

$H_{Ph\text{-}cymene}$], 5.54 [d, 2H, J(HH) = 6.2, $H_{Ph\text{-}cymene}$], 4.70 [m, 2H, C=CH_2], 3.60 [m, 2H, PCH_2], 3.09 [m, 2H, PCH_2], 2.59 [m, 1H, CHMe$_2$], 1.09 [s, 3H, Me], 0.80 [d, 6H, J(HH) = 7.0, CHMe_2]. ^{31}P{^{1}H} NMR (300 MHz, CD_2Cl_2, δ ppm): δ 28.28. MS-FAB: m/z 695.1, [Ru(p-cymene){$(Ph_2PCH_2)_2C{=}CH_2$}Cl]$^+$; 561.1, [Ru{$(Ph_2PCH_2)_2C{=}CH_2$}Cl]$^+$. Specific molar conductivity: Λ_m = 41 Ω cm^2 mol^{-1} (in ethanol).

Preparation of [Ru{p-C$_6$H$_4$(Me)(^{i}Pr)}{(Ph$_2$P)$_2$C=CH$_2$-P,P}Cl][CF$_3$SO$_3$] (2). Compound **2** was obtained following a procedure similar to that for **1** as a yellow solid, which was further purified by RP-HPLC (isocratic 100% CH_3OH, flow rate 2.0 mL/min) to give **2** (t_R = 1.7 min).

Yield: 86%. Anal. Found: C, 54.1; H, 4.3. Calcd for $C_{37}H_{36}ClF_3O_3P_2RuS$: C, 54.4; H, 4.4. IR ($\nu_{max}$/cm^{-1}): 1255s [$\nu_{as}(SO_3)$], 1223sh [$\nu_s(CF_3)$], 1155s [$\nu_{as}(CF_3)$], 1027s [$\nu_s(SO_3)$]. UV−vis [EtOH, λ_{max}, nm (ε, M^{-1} cm^{-1})]: 426 (391), 332 (1477), 220 (19681). ^{1}H NMR (300 MHz, CD_2Cl_2, δ ppm, J in Hz): δ 7.53 [m, 20H, $H_{Ph\text{-}phosphane}$], 6.50 [m, 2H, C=CH_2], 6.00 [d, 2H, J(HH) = 6.2, $H_{Ph\text{-}cymene}$], 5.86 [d, 2H, J(HH) = 6, $H_{Ph\text{-}cymene}$], 2.42 [m, 1H, CHMe$_2$], 1.64 [s, 3H, Me], 1.06 [d, 6H, J(HH) = 6.9, CHMe_2]. ^{31}P{^{1}H} NMR (300 MHz, CD_2Cl_2, δ ppm): δ 19.94. MS-FAB: m/z 667.1, [Ru(p-cymene){$(Ph_2P)_2C{=}CH_2$}Cl]$^+$. Specific molar conductivity: Λ_m = 35 Ω cm^2 mol^{-1} (in ethanol).

Crystallography. Three-dimensional, room-temperature X-ray data were collected on a Bruker X8 Apex diffractometer using graphite-monochromated Mo Kα radiation. All of the measured reflections were corrected for Lorentz and polarization effects and for absorption by semiempirical methods based on symmetry-equivalent and repeated reflections. The structures were solved by direct methods and refined by full-matrix least squares on F^2. Hydrogen atoms were included in calculated positions and refined in riding mode.

In the crystal of **2** the trifluoromethanesulfonte counterion was found to be disordered over two positions that were refined with complementary occupancies of approximately 50%.

Refinement converged with allowance for thermal anisotropy of all non-hydrogen atoms. The structure solution and refinement were carried out using the program package SHELX-97.[41]

Electrochemistry. The electrochemical experiments were performed on an EG&G Princeton Applied Research Model 273A potentiostat/galvanostat and monitored with the Electrochemistry PowerSuite v2.51 software from Princeton Applied Research. Cyclic voltammograms were obtained in acetonitrile (0.1 M) or dichloromethane (0.2 M) solutions of [NBu_4][PF_6], using a three-electrode configuration cell with a platinum-disk working electrode (1.0 mm diameter) probed by a Luggin capillary connected to a silver-wire pseudoreference electrode and a Pt-wire counter electrode. The electrochemical experiments were performed under a dinitrogen atmosphere at room temperature. The redox potentials were measured in the presence of ferrocene as the internal standard, and the redox potential values are normally quoted relative to the SCE by using the ferrocenium/ferrocene redox couple ($E_{1/2}$ = 0.40 and 0.46 V vs SCE for acetonitrile and dichloromethane, respectively). The supporting electrolyte was purchased from Fluka (electrochemical grade), dried under vacuum for several hours, and used without further purification. Reagent-grade acetonitrile and dichloromethane were dried over P_2O_5 and CaH_2, respectively, and distilled under a dinitrogen atmosphere before use.

Competitive Binding Studies. A mixture of CT-DNA (200 μM) and GelRed (20 μM, Biotium) ([CT-DNA]:[GelRed] = 10:1) were prepared in Tris-HCl 0.5 mM pH 7.0 with 50 mM NaCl. After 30 min of incubation at RT, increasing concentrations of both complexes were added to obtain [complex]:[GelRed] ratios between 1:2 and 7:1. As a control, a mixture of GelRed−CT-DNA and DMSO (same concentration as in each complex), and CT-DNA−complex mixtures without GelRed (substituting the volume of GelRed with water) were also prepared. Fluorescence emission spectra were recorded after 15 min of incubation in a CaryEcplipse fluorescence spectrophotometer (Agilent) using a 350 nm excitation wavelength, and 5 nm/5 nm slit width Ex/Em, respectively. The binding constant of both complexes to GelRed-CT-DNA complex (K_{SV}) was determined using the Stern−Volmer equation (1)

$$\frac{I_0}{I} = 1 + K_{SV}[Q] \quad (1)$$

where I_0 and I are the peak emission intensities of the GelRed−CT-DNA complex in the absence and presence of the quencher, respectively, and [Q] is the final concentration of the complex (the quencher) in each mixture.[42,43]

Cytotoxicity Assays. An assessment of cytotoxicity was evaluated by the MTT (methyl thiazolyl tetrazolium salt) assay based on the reduction of the tetrazolium salt to purple crystalline formazan by cellular mitochondrial dehydrogenases of the living cells.[44]

Three human tumor cells, A2780 ovarian MCF7 and MDA-MB-231 breast adenocarcinoma, and normal human primary fibroblasts (ATCC) were used in the assays. Cells were cultured in RPMI 1640 (A2780), DMEM + GlutaMax (MCF7, MDA-MB-231), or DMEM (fibroblasts) supplemented with 10% fetal bovine serum and 1% antibiotics at 37 °C in a CO_2 incubator. The experimental procedure followed a method similar to that previously described.[42,45] Briefly, cells ((2−5) × 10^4 cells/200 μL) were seeded in medium into 96-well plates and were allowed to adhere overnight. Complexes and ligands were first solubilized in DMSO and then in medium at serial dilutions to achieve the concentration range 100 nM to 200 μM and added to the cells (200 μL/well). After 72 h treatment with the complexes at 37 °C, the medium was replaced by 200 μL of MTT solution in PBS (0.5 mg/mL). After 3 h of incubation and solubilization of the formazan crystals that formed, the cellular viability was evaluated by measuring the absorbance at 570 nm using a plate spectrophotometer. IC_{50} was calculated using GraphPad Prism software (version 5). The selective index (SI) was calculated for each complex by dividing the IC_{50} of normal fibroblasts by the IC_{50} of tumor cells. Data (mean ± SD) was based on at least two independent experiments, each comprising six replicates per concentration.

Hoechst 33258 Labeling. MCF7 cells were collected and plated in 24-well cell culture slides at 0.75 × 10^5 cells/well. The culture medium was removed 24 h after plating and replaced with the IC_{50} of **1**, **2**, or 0.01% (v/v) DMSO (vehicle, control) diluted in fresh medium. Following 72 h of treatment, cells were stained with Hoechst 33258 (excitation and fluorescence emission 352 and 461 nm, respectively) in the absence of light for 15 min, at RT, according to the procedure previously described.[46] The samples were photographed with an Olympus BX51 fluorescent microscope with an attached Olympus DP50 (Olympus) camera, the photographs were acquired with Infarview software, and three random microscopic fields per sample with ca. 50 nuclei were counted.

Autophagic Potential. For autophagy analysis, MCF7 cells were seeded in 24-well plates at a density of at 0.75 × 10^5 cells/well diluted in 500 μL of fresh culture medium and incubated for 24 h to allow cell adherence. Cells were treated with the IC_{50} concentration of **1** or **2**. For control purposes, cells were treated with 0.01% (v/v) DMSO (negative control) or rapamycin (50 mM; positive control) for 24 h. After 72 h of incubation, the supernatants were removed, and cells were stained according to the instructions of the CYTO-ID Autophagy Detection Kit (Enzo Life Sciences, UK). Stained cells were visualized and photographed with an Olympus BX51 fluorescent microscope with an attached Olympus DP50 (Olympus) camera. Autophagy was measured using CYTO-ID Green dye (excitation and fluorescence emission 463 and 534 nm, respectively), Hoechst was used to counterstain the nucleus (excitation and fluorescence emission 358 and 461 nm, respectively) and the samples analyzed with software (ZEN Blue edition, 2011). The autophagic activity of complexes was measured through quantifying the cells with autophagolysosomes.

Cell Cycle Analysis. MCF7 cells were seeded into 8-well cell culture slides at 1 × 10^5 cells/mL, incubated for 24 h at 37 °C, 99% (v/v) humidity, and 5% (v/v) CO_2, and synchronized in early S-phase by a double thymidine block (2 mM; Sigma, St. Louis, MO, USA) as described before.[47] Cells were released from the second block by substituting with fresh medium containing the IC_{50} concentration of

https://dx.doi.org/10.1021/acs.inorgchem.0c02768
Inorg. Chem. 2021, 60, 2914−2930

1, **2**, or 0.01% (v/v) DMSO (vehicle, control) and was left to incubate for 6, 9, 12, and 24 h at 37 °C and 5% (v/v) CO_2. For synchronization control purposes, cells from another disk were collected after the thymidine block. After each time point, cells were trypsinized with TrypLE Express and centrifuged for 5 min at 650*g* at 4 °C. Supernatants were removed, and the pellets were resuspended in PBS 1x. An additional centrifugation was performed under the previously mentioned conditions. The cell pellet was resuspended in PBS 1x and ethanol 80% (v/v) in a proportion of 1:10. Ethanol solution was added cautiously with constant vortex. Cells were stored at 4 °C for at least 12 h. After incubation, cells were centrifuged for 10 min at 5000*g* at 4 °C and the pellets were treated with 50 μg/mL RNase A for 30 min at 37 °C and then with PI (25 μg/mL). The DNA content was analyzed on an Attune Acoustic Focusing Flow Cytometer (Applied Biosystems), and the data collected were treated with FCS Express 6 Flow Cytometry software.

Intracellular Reactive Oxygen Species (ROS). Reactive oxygen species (ROS) Detection Reagents (Life Technologies, Invitrogen, USA) were used to detect the accumulation of mitochondrial generated intracellular ROS.[48] MCF7 cells were seeded into 24-well cell culture slides at 0.75×10^5 cells/well density and incubated for 24 h at 37 °C, 99% (v/v) humidity, and 5% (v/v) CO_2. Afterward, the medium was removed and replaced by fresh medium containing 3 × IC_{50} concentration of **1**, **2**, or 0.01% (v/v) DMSO (vehicle, control). Additionally, hydrogen peroxide (H_2O_2) at a concentration of 50 μM was used as a positive control. After 24 h, cells were washed gently three times with PBS 1x, stained with 10 μM of H_2DCF-DA in prewarmed PBS 1x, and incubated at 37 °C for 20 min, protected from light. The unbound H_2DCF-DA was removed by washing the cells two times with PBS 1x. Samples were observed in a Ti-U Eclipse inverted microscope (Nikon, Tokyo, Japan), and images were acquired using NIS Elements Basic software (Nikon). The relative fluorescence intensity of DCF was measured using ImageJ software.

Cellular Uptake. For cellular uptake, MCF7 cells were collected and plated in 24-well cell culture slides at 1×10^5 cell/mL. The culture medium was removed 24 h after plating and replaced with 10 × IC_{50} concentration of **1** or **2** diluted in fresh medium. Following 3 h of treatment (4 or 37 °C), culture supernatants were recovered and centrifuged at 700*g* for 5 min to recover cells in suspension. Adherent cells were harvested with TrypLE Express and centrifuged at 700*g* for 5 min. Both cell pellets were washed twice with ice-cold PBS, and the respective cell pellets were collected by centrifugation at 700*g* for 5 min. The cell pellets were resuspended in 1 mL of fresh *aqua regia*. All samples were analyzed by inductively coupled plasma atomic emission spectroscopy (ICP-AES) (Laboratory of analyses, service of atomic emission spectroscopy, Department of Chemistry, FCT-UNL), to determine the amount of metal (Ru) present in the samples.

Statistical Analysis. All data were expressed as mean ± SEM from at least three independent experiments. The statistical significance was evaluated using the Student *t* test; $p < 0.05$ was considered statistically significant. Statistical analysis was performed using GraphPad Prism v6.01 (GraphPad Software, La Jolla, CA, USA).

Interaction with Human Serum Albumin (HSA). Steady-state fluorescence measurements were carried out at room temperature on a Spex FL-1057 Tau 3 spectrofluorometer from Horiba Jobin Yvon. In these experiments, Millipore water was used for the preparation of 10 mM solutions of 4-(2-hydroxyethyl)-1-piperazineethanesulfonic acid (Hepes) buffer (from Sigma-Aldrich), and the buffer pH was adjusted to 7.4 with KOH and/or HCl (4 M) solutions.

Stock solutions of human serum albumin (HSA from Sigma-Aldrich) were prepared by gently dissolving the protein in Hepes buffer (pH 7.4, 10 mM) for about 30−60 min to allow the protein to hydrate and fully dissolve, being gently swirled from time to time. The concentration of each HSA stock solution was determined by UV spectrophotometry using the molar extinction coefficient ε(278 nm) = 36850 M^{-1} cm^{-1}.[49] Individual protein−complex samples were prepared to ensure the same incubation time in each assay. The final protein concentration in all samples was 2 μM, and the complex concentration was varied accordingly to obtain HSA:Ru complex molar ratios ranging from 1:0.5 to 1:4 (for complex **1**) and 1:1.5 to 1:8 (for complex **2**). Samples with the same concentration of the complex but with no protein were prepared for appropriate background correction.

The excitation wavelength was 295 nm, and the fluorescence emission intensity was corrected for absorption and emission inner filter effects using UV−vis absorption data recorded for each sample.[42,50] For both complexes, the high overlap between their absorption spectra and the HSA-Trp214 emission spectrum makes it possible for reabsorption of emitted light. These inner filter effects and reabsorption of light (which are not due to a real interaction) both decrease the protein fluorescence intensity, and hence data must be corrected for these features.[42,43]

DMSO (from Sigma-Aldrich, spectroscopic grade) was used to prepare concentrated stock solutions of each complex, following an appropriate dilution (in DMSO and buffer) to obtain the desired complex concentration and the same 2% (v/v) DMSO in the final samples. All stock solutions were prepared (and dilutions carried out) immediately prior to sample preparation. Individual samples were prepared and incubated overnight (about 18 h) at 37.0 ± 0.1 °C to ensure that equilibrium was fully attained before measurements. Binding constants were estimated from Stern−Volmer linear/quadratic data fits (of two independent experiments).[42,43]

Fish Embryo Acute Toxicology Test (FET). *Ethical Statement.* Toxicity studies *in vivo* using zebrafish embryos do not fall under the regulation of European Directive 2010/63/EU on the protection of animals used for scientific purposes.[51] In addition, according to the European Food Safety Administration,[52] these studies comply with the principles[53] for humane animal research.

Adult zebrafish (*Danio rerio*) individuals were kept under standard conditions[44] in tanks containing dechlorinated tap water, being fed with dry flakes and *Artemia* sp. twice and once a day, respectively. To obtain fertilized eggs, fish were transferred to mating tanks in a 2:1 female to male ratio. The next morning, eggs were rinsed and collected in Petri dishes containing sterile dechlorinated tap water (SDTW). Fertilized eggs were used to test the toxicity of **1** and **2** following FET guidelines[39] with a few modifications. The final concentrations tested were 25, 17.5, 10, 7.5, 5, and 2.5 μM for **1** and 40, 20, 15, 10, and 5 μM for **2**. Because of the relatively low solubility of the complexes, all solutions contained 0.5% DMSO in SDTW.[53] In addition, various controls were also tested: (A) negative control and internal plate control (SDTW; embryo mortality <10%); (B) solvent control (0.5% DMSO in SDTW; embryo mortality <10%); (C) positive control (4.0 mg/L 3.4-dichloroaniline solution; embryonic mortality >30%). All tested solutions had a conductivity of 190.0 ± 60.0 μS/cm and pH 7.4 ± 1. Four replicates were performed for each compound. In each experiment, 12 embryos at the early blastula stage (2.5−3 h postfertilization (hpf)) were exposed to each solution in a static system maintained at 26 ± 1 °C. The acute toxicity was analyzed every 24 h up to 96 hpf, recording five end points based on FET guidelines:[39] (a) coagulated embryos; (b) presence of edema; (c) absence of somite formation; (d) nondetachment of the tail from the yolk sac, and (e) lack of heartbeat after 48 hpf. Although not an end point, hatching was also monitored as a sign of exposure of the embryo to the tested complexes. After experiments were completed, the surviving larvae were euthanized. All experiments were done following the recommendations of Spanish (RD 53/2013) and European (EU 2010/63) regulations.

Lethal concentration values at which 50% of the embryos show signs of acute toxicity (LC_{50}) were determined by logistic regression and interpolation analyses with data obtained at 96 hpf. Data are expressed as mean ± standard error of the mean from four independent experiments. Statistical analyses were performed using Excel 2016 (Microsoft) and SPSS (IBM). Graphs showing mortality response curves were represented using Graph Prism software.

RESULTS AND DISCUSSION

Treatment of commercially available $[Ru(p\text{-cymene})(Cl)(\mu\text{-}Cl)]_2$ with silver triflate and the corresponding phosphane

https://dx.doi.org/10.1021/acs.inorgchem.0c02768
Inorg. Chem. 2021, 60, 2914−2930

coligand in dichloromethane under argon yielded complexes **1** and **2** (see Scheme 1). The difference between them lies in the

Scheme 1. Structure of the [Ru(*p*-cymene)(L)Cl]$^+$ Complexes Prepared and Isolated as the Corresponding Triflate Salt[a]

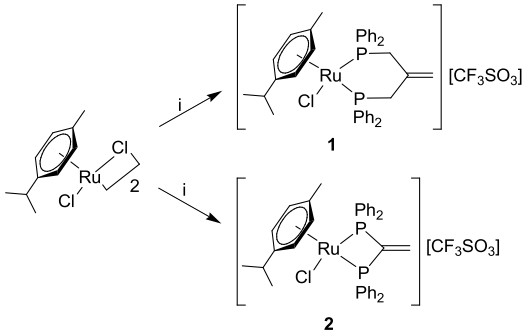

[a]Legend: (i) (1) $AgCF_3SO_3$ (2 equiv)/dichloromethane, (2) **L** (1 equiv)/dichloromethane, with **L** being 1,1-bis-(methylenediphenylphosphano)ethylene (**L1**) for **1** and 1,1-bis-(diphenylphosphano)ethylene (**L2**) for **2**.

presence of a methylene group in the phosphane coligand in the case of compound **1** that is localized between phosphorus atoms and the terminal double bond (see Scheme 1) with the phosphane coligand forming a six-membered chelate in **1** and a four-membered chelate in **2**. The complexes were isolated as air-stable solids in very good yields (ca. 85%) and were fully characterized (see the Experimental Section).

The analytical data were consistent with the structures proposed, and MS FAB spectra showed *m*/*z* values and isotopic pattern distributions in agreement with the those expected for [Ru(*p*-cymene)(L-L)Cl]$^+$, i.e. the product ion [M − (CF_3SO_3)]$^+$, thereby confirming the mononuclear nature of these complexes. The values of conductivity data were in accordance with those observed in 1:1 electrolytes (35−41 Ω cm^2 mol^{-1} in ethanol).[54] In the IR spectrum of **1** and **2** four bands between 1270 and 1020 cm^{-1} were assigned to the characteristic asymmetric and symmetric stretching modes of SO_3 and CF_3 groups and were consistent with the presence of the triflate counterion.[55]

The $^{31}P\{^1H\}$ NMR spectra for complexes **1** and **2** showed singlets at 28.28 and 19.94 ppm, respectively, confirming that the two phosphorus nuclei were equivalent (see Figure S1 in the Supporting Information).[56] The ^{31}P chemical shifts were influenced by ring size.[57] The six-membered ring in compound **1** gave a positive Δ_R value, +7.7, in contrast with an equivalent phosphorus in a nonchelated analogue, [Ru(*p*-cymene)-$(PPh_3)_2Cl)](BF_4)$, in which $\delta(P)$ = 21.1 ppm,[58] whereas the four-chelate ring in compound **2** gave a slightly negative Δ_R value (−0.6).

In the ^1H NMR spectra of both complexes (see Figure S2) the H_{phenyl} resonances of the coordinated *p*-cymene ligand were observed as a pattern of two doublets at ca. 6.00 ppm. The doublet at ca. 1.00 ppm was assigned to the $CHMe_2$ resonance, and a singlet at 1.1−1.2 ppm was assigned to the three methyl protons of the *p*-cymene ligand. Finally, $CHMe_2$ was observed as a multiplet at ca. 2.5 ppm. The difference between the compounds is the presence of the methylene group in the phosphane coligand in the case of compound **1**. The H_{phenyl} resonances of the diphosphane ligands were detected at ca. 7.50 ppm. In the case of compound **1** the signal of the vinyl group in the phosphane was detected as a singlet at 4.70 ppm, while in the case of complex **2** the vinyl group is detected as a multiplet at 6.50 ppm due to the coupling of the vinyl protons with the phosphorus atoms. For complex **1**, H−P coupling was also observed in the multiplet assigned to the methylene group and detected in the 2.5−3.0 ppm range. In addition, the presence of the phenyl groups in the phosphane ligand resulted in an upfield-shifted resonance for the Me_{cymene} group, which was assigned as a singlet at ca. 1.20 ppm.

X-ray Crystallographic Study. Single crystals suitable for X-ray diffraction were obtained by slow solvent evaporation from dichloromethane/*n*-hexane solutions of complexes **1** and **2**. Significant crystallographic data are given in Table 1 and selected bond distances and angles in Table 2.

Table 1. Crystal Data and Structure Refinement Details for Compounds 1 and 2

	1	2
formula	$C_{40}H_{42}Cl_3F_3O_3P_2RuS$	$C_{37}H_{37}ClF_3O_{3.50}P_2RuS$
FW	929.16	825.19
cryst syst	triclinic	monoclinic
space group	$P\bar{1}$	$P2_1/n$
a (Å)	11.825(7)	11.514(6)
b (Å)	12.103(9)	10.559(7)
c (Å)	15.847(4)	28.951(8)
α (deg)	107.788(7)	
β (deg)	107.421(9)	91.978(9)
λ (deg)	95.574(9)	
V (Å^3)	1987(2)	3518(3)
Z	2	4
μ (mm^{-1})	0.782	0.726
max, min transmission	0.7937, 0.7349	0.8684, 0.7173
θ range (deg)	1.45−28.36°	1.88−30.65
no. of rflns collected	154955	116429
no. of unique rflns	9913	10878
R_{int}	0.0289	0.0374
R1[a]	0.0275	0.0230
wR2[b]	0.0855	0.0739

[a]$R1 = \sum||F_o| - |F_c||/\sum|F_o|$, $F > 4\sigma(F)$. [b]$wR2 = [\sum[w(F_o^2 - F_c^2)^2/\sum w(F_o^2)^2]]^{1/2}$, all data.

Table 2. Selected Bond Lengths (Å) and Angles (deg) for Compounds 1 and 2

	1	2
Ru(1)−Cl(1)	2.386(1)	2.388(1)
Ru(1)−P(1)	2.320(1)	2.311(1)
Ru(1)−P(2)	2.329(1)	2.320(1)
C(1)−C(2)		1.333(2)
C(2)−C(4)	1.331(3)	
P(1)−Ru(1)−P(2)	90.59(5)	72.37(3)
P(1)−Ru(1)−Cl(1)	83.00(3)	83.63(3)
P(2)−Ru(1)−Cl(1)	84.08(4)	83.74(4)

Crystals of **1** and **2** consist of one molecular cation, one trifluoromethanesulfonate anion, and (in the crystal of **1**) one dichloromethane solvent molecule per asymmetric unit.

The complexes show the typical "piano-stool" structure with the Ru(II) atom coordinated to the η^6-*p*-cymene, to a chlorine ligand, and to the chelating P,P ligand (tertiary diphosphane) (see Figure 2).

https://dx.doi.org/10.1021/acs.inorgchem.0c02768
Inorg. Chem. 2021, 60, 2914−2930

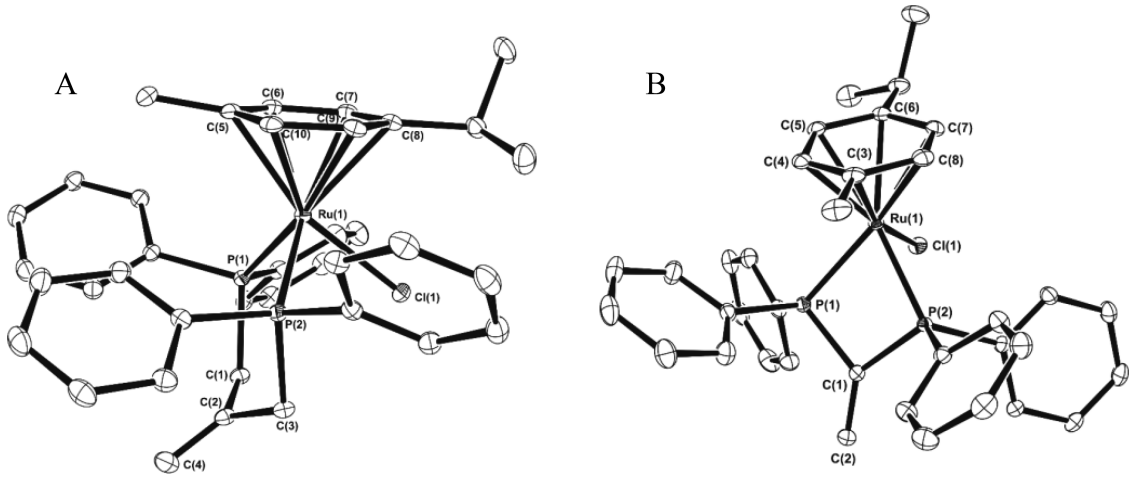

Figure 2. Molecular structures for the cation of compound **1**, $[Ru\{p\text{-}C_6H_4(Me)(^iPr)\}\{(Ph_2PCH_2)_2C{=}CH_2\text{-}P,P\}Cl]^+$ (A), and the cation of compound **2**, $[Ru\{p\text{-}C_6H_4(Me)(^iPr)\}\{(Ph_2P)_2C{=}CH_2\text{-}P,P\}Cl]^+$ (B). Ellipsoids are drawn at the 50% probability level. Hydrogen atoms have been omitted for clarity.

In complex **1** the six-membered chelate ring shows a boat conformation with the metal and C(2) carbon atoms above and below the plane formed by P(1), P(2), C(1), and C(3). However, in complex **2** the four-membered chelate is almost planar.

In both complexes, the coordination plane P(1)−Ru(1)−P(2) forms angles with the *p*-cymene aromatic ring of 63.7 and 45.0° for **1** and **2**, respectively, in order to relieve the steric hindrance.

The P(1)−Ru(1)−P(2) bond angle is considerably larger in complex **1** than in complex **2** (90.6(1)° compared to 72.4(1)°) due to the greater strain of the four-membered chelate ring (C(1),P(1),Ru(1),P(2)) formed by the phosphane ligand in **2**. However, the Ru(1)−P bond distances (within the 2.311(1)−2.329(1) Å range) are almost identical in both complexes, indicating that the greater chelate strain in **2** does not debilitate the Ru−P bonds. Ru(1)−Cl(1) bond distances are similar in both complexes (2.3857(7) and 2.3876(9) Å for **1** and **2**, respectively), showing the small influence of the coordination environment on the Ru−Cl bond strength. All bond lengths and angles agreed with previously reported values.[59]

Electrochemical Studies. The electrochemical behavior of complexes **1** and **2** as well as that of the corresponding free phosphane coligands **L1** and **L2** was studied by cyclic voltammetry by scanning the potential between the solvent experimental limits at a scan rate of 200 mV s^{-1}. Measurements were performed at a platinum-disk electrode (WE) in acetonitrile and dichloromethane solutions containing tetrabutylammonium hexafluorophosphate (0.1 and 0.2 M, respectively).

Figure 3 shows the electrochemical profiles for complexes **1** and **2** in acetonitrile, and electrochemical data are presented in Table S1 and Figures S4 and S5 in the Supporting Information.

In acetonitrile, ligands **L1** and **L2** show irreversible oxidations in the positive potential range at E_{pa} = 1.06 V and E_{pa} = 1.29 V, respectively, and their behavior is quite similar in dichloromethane (Figure S4). With regard to the redox behavior of complexes **1** and **2**, in acetonitrile (a polar and coordinating solvent) both complexes exhibit one oxidation process associated with the Ru(II)/Ru(III) couple upon scanning toward positive potentials. On the return scan, the reduction wave of the same redox couple was observed for

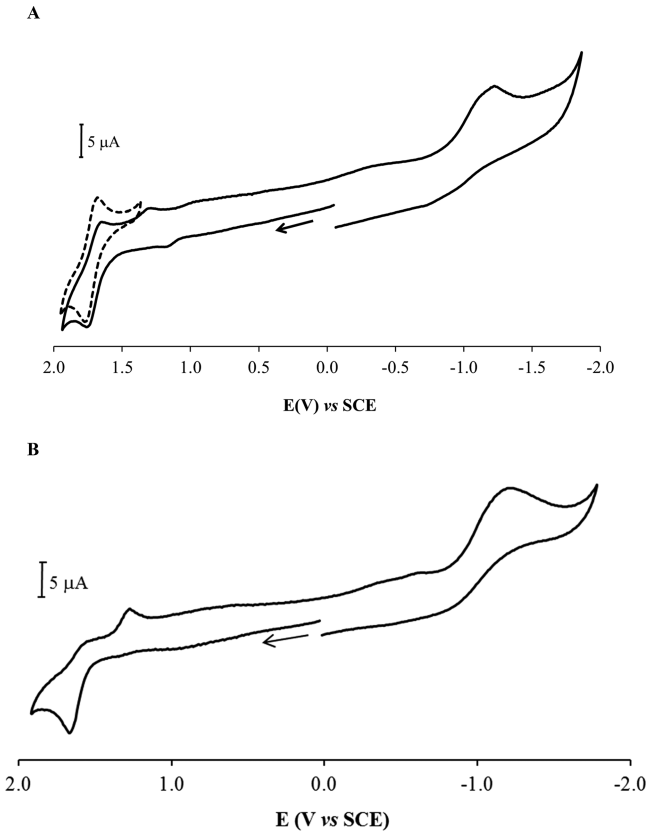

Figure 3. Cyclic voltammogram of complex **1** (A) and complex **2** (B) in acetonitrile (scan rate 200 mV s^{-1}).

complex **1**, corresponding to a quasi-reversible process with $E_{1/2}$ = 1.71 V (Figure 3A). For complex **2**, the Ru(II)/Ru(III) process becomes irreversible (E_{pa} = 1.67 V), even when it is isolated and studied at different scan rates, which indicates that the oxidized Ru(III) species is not stable and is probably involved in further irreversible chemical and/or electron-transfer reactions (Figure 3B). The Ru(II) center in complex **2** is more easily oxidized than in **1**, which indicates that the ligand **L2** is a better electron donor than **L1**, as a lower Ru(II)/Ru(III) potential can be associated with a stronger σ-

https://dx.doi.org/10.1021/acs.inorgchem.0c02768
Inorg. Chem. 2021, 60, 2914−2930

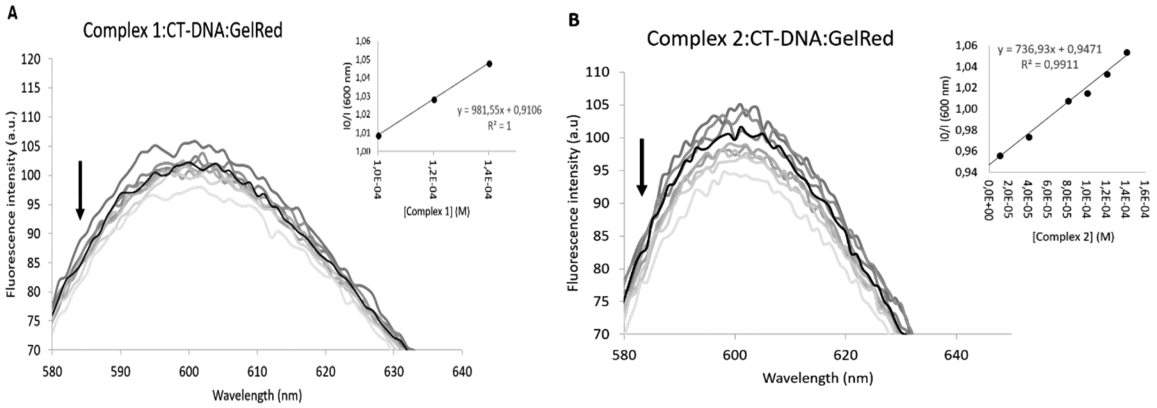

Figure 4. Absorption spectra of the competitive reaction between different ratios of compounds **1** (A) and **2** (B) and GelRed bonded to CT-DNA: [GelRed] = 20 μM and [CT-DNA] = 200 μM in 0.5 mM Tris/HCl pH 7.0 with 50 mM NaCl. The black arrow indicates the quenching effect observed with an increasing concentration of complexes. Insets: plots of I_0/I vs [complex] and the corresponding linear fits.

donating ability of the ligand. Both complexes also show ligand-based irreversible reduction processes at −1.22 and −1.21 V, respectively.

In dichloromethane, complex **2** showed a behavior similar to that in acetonitrile (see Figure S5 in the Supporting Information). The oxidation process around 1.6 V, when it was isolated and studied at different scan rates, was shown to be irreversible, suggesting that a rapid and irreversible chemical reaction follows the electron transfer process. Also, the redox behavior of complex **1** (see Figure S5 in the Supporting Information) is quite complex, with a profile compatible with successive chemical processes. Upon scanning toward positive potentials, complex **1** showed an oxidation process for the Ru(II) center at around 2.0 V with a small reduction process observable upon back-scanning around 1.82 V. Scan reversal following the Ru(II)/Ru(III) oxidation shows two new small reduction peaks at 1.03 and 0.84 V, respectively. This behavior indicates that the oxidized Ru(III) compound is not stable in this solvent, being involved in further chemical and/or electron-transfer reactions. The complex also shows an adsorption peak at 0.19 V and a ligand-based irreversible reduction process at −1.04 V. The noncoordinative nature and the low polarity of this solvent, minimizing the solvent−complex interactions, could be responsible for the different behavior observed in acetonitrile and dichloromethane. The appreciably high Ru(II)/Ru(III) potentials and the irreversible nature of the oxidation processes found for these complexes indicate the formation of unstable ruthenium(III) species on the cyclic voltammetric time scale, or in other words, the ligand field environment around the metal ion is suitable to stabilize the ruthenium(II) state.

UV−Visible and Complex Solubility and Stability in Aqueous Media. The complexes are highly soluble in ethanol and in nonprotic solvents such as dichloromethane, acetone, and DMSO. UV−vis spectra of the complexes were recorded at room temperature in $\sim 10^{-4}-10^{-6}$ M ethanol solutions under the same experimental conditions. The electronic spectra (see Figure S3 in the Supporting Information) showed a very intense band ascribed to $\pi-\pi^*$ electronic transitions occurring in the organometallic fragment Ru(*p*-cymene) (λ 200−270 nm), a weak band assigned to metal−ligand charge-transfer transitions (MLCT) from Ru 4d orbitals to the π^* orbitals of the ligands (λ 290−390 nm), and a shoulder assigned to d−d transitions (λ 400−600 nm), as has been reported in similar arene complexes.[60]

The stability of complexes **1** and **2** in solution was evaluated over time by monitoring their UV profiles over a period of 24 h at room temperature (using 2−4% of DMSO to fully dissolve the complexes in aqueous media and cell culture media DMEM). Both complexes demonstrated a good stability in aqueous solution with minimal changes in their UV−visible spectra (see Figures S6−S8 in the Supporting Information). This stability was confirmed by $^{31}P\{^1H\}$ NMR spectroscopy in dmso-d_6, where no change was observed up to 72 h.

Competitive DNA Binding Studies. Binding studies of Ru(II) complexes with DNA are important in the design of new drugs that target DNA. Competitive DNA binding is a technique (often used) to study the interaction between drugs and DNA. It is well-known that GelRed is an indicator for intercalation of DNA, and this molecule forms a soluble complex with nucleic acids.[61] The extent of DNA binding is directly related to the percentage of fluorescence decrease. The binding of complexes **1** and **2** to CT-DNA with GelRed as a competitive intercalative binding probe was analyzed. In competitive binding experiments, GelRed was first incubated with CT-DNA for 30 min to ensure that the interaction between DNA and GelRed was complete (the concentration ratio was set at [GelRed]:[CT-DNA] = 1:10). The emission spectra of the GelRed−CT-DNA system in the absence and presence of increasing concentration of complexes **1** and **2** are shown in Figure 4.

As seen in Figure 4 it is noteworthy that, on excitation at 350 nm, the GelRed−CT-DNA system presents a characteristic fluorescence emission at around 590 nm. The addition of both complexes induced a small quenching of the emission band of the GelRed−DNA system, indicating some competitive effect of both complexes with GelRed for CT-DNA intercalation. However, this decrease in fluorescence intensity (observed with a 7:1 ratio of complex:GelRed) is lower in comparison to other compounds that are known to compete with GelRed for DNA intercalation.[62] The quenching constants (K_{SV}) for complexes **1** and **2** bound to GelRed−DNA system were determined to be 9.8×10^2 and 7.4×10^2 M^{-1}, respectively, values that are indeed lower than expected for an effective competitive effect.

Cell Studies: Cytotoxicity in Human Tumor and Normal Cell Lines. The cytotoxicities of complexes **1** and **2** were assessed in human ovarian carcinoma (A2780) and breast adenocarcinoma (MCF7 and MDA-MB-231, hormone-dependent and hormone-independent (triple negative) cell lines,

https://dx.doi.org/10.1021/acs.inorgchem.0c02768
Inorg. Chem. 2021, 60, 2914−2930

Table 3. IC_{50} Values (μM) Calculated from Dose−Response Plots Obtained for Complexes 1 and 2 upon 72 h Treatment[a]

	IC_{50} (μM)				SI		
	A2780	MCF7	MDA-MB-231	fibroblasts	A2780	MCF7	MDA-MB-231
1	0.32 ± 0.17	0.19 ± 0.05	0.40 ± 0.21	8.1 ± 1.3	25.3	42.6	20.25
2	1.87 ± 0.59	1.54 ± 0.50	2.56 ± 0.75	4.4 ± 0.9	2.3	2.8	1.7

[a]Data shown are the averages of at least three replicates; standard deviation values are indicated. Definitions: A2780, human ovarian adenocarcinoma; MCF7, human hormone-dependent breast adenocarcinoma; MDA-MB-231, human triple-negative breast adenocarcinoma. The selectivity index (SI) was calculated for each cell line toward fibroblasts.

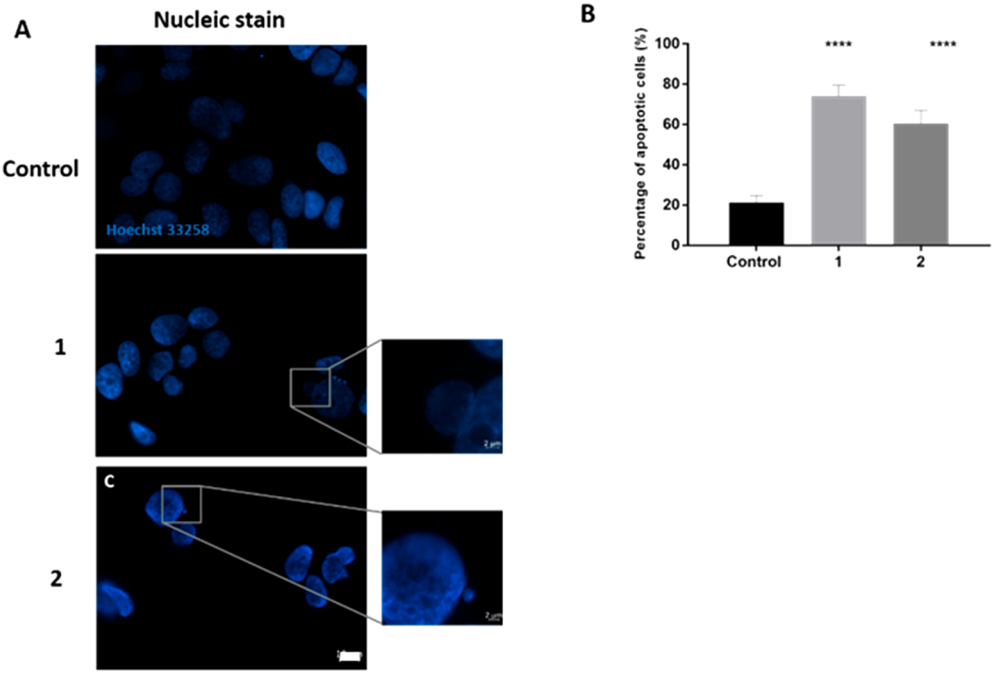

Figure 5. (A) Hoechst staining of the MCF7 cell line for an analysis of apoptotic nuclei (excitation and fluorescence emission spectra 352 and 461 nm, respectively). Cells were grown in DMEM culture medium supplemented with 10% fetal bovine serum in the presence of 0.01% (v/v) DMSO control and complexes **1** and **2** (at IC_{50}). The insets show chromatin condensation and apoptotic bodies characteristic of apoptosis. Plates were photographed with an AXIO Scope (Carl Zeiss, Oberkochen, Germany). Two random microscopic fields per sample with ca. 50 nuclei were counted. (B) Percentage of apoptosis in MCF7 cells exposed to 0.01% DMSO and IC_{50} of each complex. Data are expressed as means ± SEM of three independent assays (***$p \leq 0.001$, ****$p \leq 0.0001$). The scale bar corresponds to 10 μm.

respectively) and in normal human primary fibroblasts. Cells were treated with different concentrations of the complexes in the range 100 nM to 200 μM over 72 h, at 37 °C. IC_{50} values were calculated from dose−response curves obtained using the MTT assay (see Figure S9 in the Supporting Information).

The complexes were first solubilized in DMSO and then in the cell culture medium, keeping the percentage of DMSO at the highest concentration which induced no cytotoxic effect, 1%. The phosphane coligands were evaluated in the same concentration range of the complexes for comparison, presenting no cytotoxicity (IC_{50} > 100 μM) in all tumor cell lines investigated.

The results showed that coordination to the "Ru(*p*-cymene)" moiety is highly beneficial for the biological activity of complexes **1** and **2** (Table 3), the trend against the carcinoma cells being **1** ≫ **2**. In fact, complex **1** displayed a remarkable cytotoxicity in the submicromolar concentration range even for the triple-negative MDA-MB-231 breast cells, known for their very aggressive phenotype.

Despite both complexes displaying cytotoxic activity in normal human primary fibroblasts (Table 3; see Figure S10 in the Supporting Information), IC_{50} values are much higher in comparison to those found in tumor cells. Complex **1** showed a much higher selectivity index (SI) toward cancer cells in comparison to complex **2** (Table 3), with an IC_{50} that is 20× or 25× higher in nontumor cells in comparison with its IC_{50} in MDA-MB-231 or A2780 cells and 43× higher than the respective value for MCF7 cells. In contrast, complex **2** displayed an IC_{50} 2× higher and 3× higher for noncancer cells in comparison to its IC_{50} in A2780 and MCF7 cells, respectively.

Except for Ru(arene) compounds bearing the phosphaadamantane PTA coligand that have been shown as promising anticancer metallodrugs,[13] cytotoxic studies based on half-sandwich ruthenium arene compounds with other phosphane ligands are scarce in the literature. Nevertheless, examples bearing the cyclopentadienyl scaffold can be found.[11,63] Most complexes of this family exhibit interesting cytotoxic activity that is modulated by the set of coligands. $[Ru(C_5H_5)(dppe)(4\text{-Me-py})][PF_6]$ (C_5H_5 = η^5-cyclopentadienyl; dppe = 1,2-bis(diphenylphosphino)ethane; 4-Me-py = 4-methylpyridine) showed a high antiproliferative activity against the leukemia cell line HL-60, as did the complex $[Ru(C_5H_5)(PPh_3)(bpy)][CF_3SO_3]$ (PPh_3 = triphenylphosphane; bpy = 2,2′-bipyridine).[11] The latter complex was also found to be active in the submicromolar range against several cisplatin-resistant

https://dx.doi.org/10.1021/acs.inorgchem.0c02768
Inorg. Chem. 2021, 60, 2914−2930

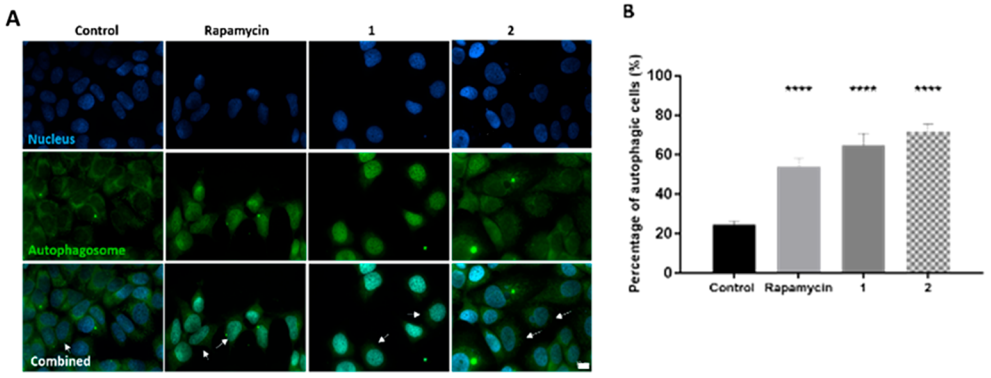

Figure 6. (A) Autophagic cell death evaluation using the CYTO-ID Autophagy detection assay in the presence of 0.01% (v/v) DMSO (vehicle control), rapamycin (as an autophagy marker), and complexes **1** and **2** and assessed by fluorescence microscopy. Nuclei were stained with Hoechst (excitation and fluorescence emission 358 and 461 nm, respectively), and autophagosomes were stained in green (excitation and fluorescence emission 463 and 534 nm, respectively). White arrows point to cells with autophagosomes. Plates were photographed with an AXIO Scope (Carl Zeiss, Oberkochen, Germany). (B) Percentage of autophagic MCF7 cells exposed to 0.01% DMSO and IC_{50} of each complex. Data are express as means ± SEM of three independent assays (***$p \leq 0.001$). The scale bar corresponds to 10 μm.

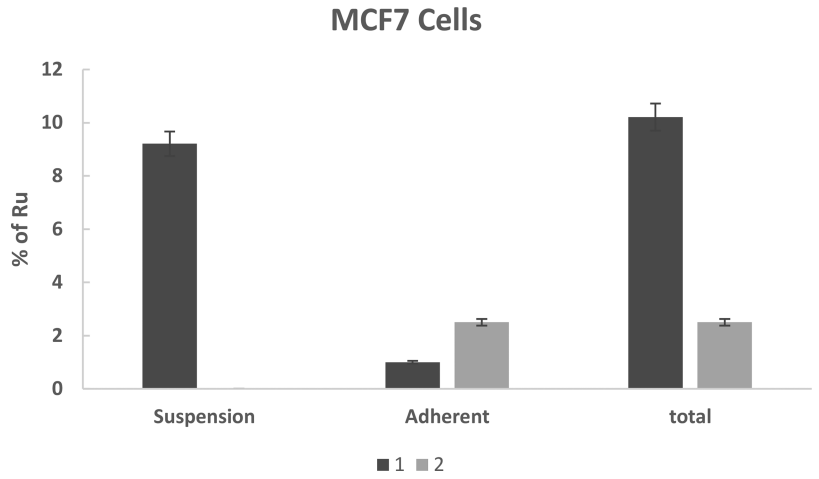

Figure 7. Percentage of intracellular ruthenium in MCF7 cells (total, adherent, suspension) after exposure to compounds **1** and **2**. The metal content was determined by ICP-AES after an incubation time of 3 h at 37 °C with 10 × IC_{50} concentration of both complexes, corresponding to 1.9 μM for compound **1** and 15.4 μM for compound **2.** Data are expressed as means ± SEM of two independent assays, and the statistical significance was evaluated by a nonparametric *t* test (**$p \leq 0.01$).

cells,[42,64] and the presence of the phosphane ligand in the coordination sphere of the "Ru(C_5H_5)" moiety was found to be absolutely essential for the cytotoxic activity of these complexes.[65] Recently, high activity toward cancer cells with IC_{50} values in the micromolar range has also been reported for polymer−ruthenium−cyclopentadienyl derivatives with PPh_3.[66] Since Ru(*p*-cymene) complexes are typically found to be less active against tumor cells than e.g. Ru-(cyclopentadienyl) derivatives, our results suggest that the inclusion of a chelated diphosphane ligand is a suitable approach to increase the cytotoxic activity in these Ru-based compounds. Indeed, the activity reported for [Ru(*p*-cymene)-{1,1-bis(diphenylphosphanomethane-*P*}Cl_2] with a monodentate diphosphane ligand is lower against the MCF7 cell line (IC_{50} = 2.6 μM).[67]

Apoptosis and Autophagy. On the basis of the cytotoxic results of both complexes in MCF7, the cell model with the lowest IC_{50} found, their ability to induce apoptosis was analyzed via Hoechst 33258 (2′-[4-ethoxyphenyl]-5-[4-methyl-1-piperazinyl]-2,5′-bi-1*H*-benzimidazole trihydrochloride trihydrate) staining.[68] As depicted in Figure 5, an increase of apoptotic markers was observed, such as chromatin condensation and apoptotic bodies, corresponding to 74 ± 5% of apoptotic cells for complex **1** (a 3.5-fold increase over the control) and 60 ± 6% of apoptotic cells for complex **2** (3-fold increase over the control).

Despite the morphological changes observed, other types of programmed cell death (PCD) might also be occurring, such as type II autophagic cell death as previously observed with other Ru(II) complexes.[9,35] In this type of cell death, portions of the cell are enclosed in double-membrane vesicles called autophagosomes that fuse with lysosomes, forming autophagolysosomes, for protease degradation.[69] Cells exposed to complexes **1** and **2** showed an accumulation of autophagolysosomes characteristic of the induction of autophagy (see Figure 6), with 65 ± 6% of autophagic cells for complex **1** (which translates into a 2.6-fold increase over the control (DMSO)) and 70 ± 4% of autophagic cells for complex **2** (2.8-fold increase over the control).

Our data demonstrated that cell exposure to these complexes induces both the hyperactivation of autophagy and the induction of apoptosis, thus leading to death of the cancer cells. These results suggest that complexes **1** and **2**

https://dx.doi.org/10.1021/acs.inorgchem.0c02768
Inorg. Chem. 2021, 60, 2914−2930

might offer new treatment options to overcome resistance to apoptosis in cancer cells.[70]

Internalization of Ruthenium Complexes. Cellular internalization of Ru(II) complexes in adherent MCF7 cells was first accessed after incubation of complexes **1** and **2** at the IC_{50} concentration for 72 h. However, by using this concentration we were not able to determine any Ru in the samples (below the limit of detection of Ru by ICP-AES). We next tested a higher concentration (10 × IC_{50}, corresponding to 1.9 and 15.4 μM of complexes **1** and **2**, respectively) but with a lower exposure time to the complexes (3 h, due to complex cytotoxicity) and the percentage of Ru was analyzed by ICP-AES. As observed in Figure 7, an average of 1% of complex **1** and 2.5% of complex **2** is taken up by adherent MCF7 cells within 3 h of incubation at 37 °C, meaning that both complexes can enter cells. Interestingly, when we compare the internalization at 4 °C the percentage of internalized Ru was the same (results not shown), indicating that both complexes are able to enter the cells in the absence of energy, thus they enter by passive transport.

Considering the higher cytotoxicity of complex **1**, we were expecting to observe a higher percentage of Ru in adherent MCF7 cells exposed to **1** in comparison to **2**. However, this was not observed in adherent cells (Figure 7). Considering this result, we decided to analyze the presence of cells in the culture supernatant after exposure to complex **1** or **2**. In fact, while complex **1** was able to induce cell detachment from the T-flask, the same effect was not observed in the presence of complex **2**. Indeed, when we measured the percentage of Ru in the fraction of cells in suspension after treatment with complex **1**, we were able to find a very high percentage (9.2%) of Ru (Figure 7). When we consider the total percentage of Ru in MCF7 cells (adherent + suspension) we observed 5× more complex **1** inside cells in comparison to complex **2** (10.2% versus 2.5%) (Figure 7). These results agree with the cytotoxicity data **1** > **2** previously presented.

Reactive Oxygen Species (ROS) Induction. One of the mechanisms that is related to apoptosis induction is the generation of reactive oxygen species by metal complexes.[71] Considering this, we have assessed the effect of both complexes in ROS induction (Figure 8). As observed, there is an increase in the production of ROS when cells were incubated with 3 × IC_{50} of each complex for 24 h. Indeed, intracellular ROS levels observed are higher for both complexes in comparison to the positive control (H_2O_2) (Figure 8).

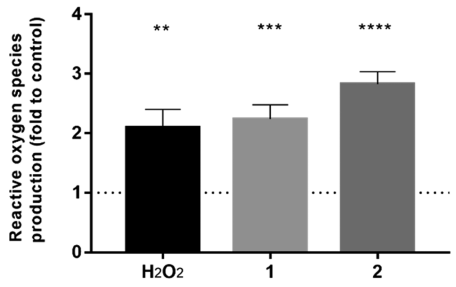

Figure 8. Quantification of the fluorescence intensity of H_2DCF-DA dye in MCF7 cells after exposure to hydrogen peroxide (H_2O_2, 50 μM), 0.1% v/v DMSO (vehicle control), or complexes **1** and **2** (at 3 × IC_{50}) for 24 h. Results are the mean ± SEM of two independent experiments and are normalized to control cells (0.1% v/v DMSO). The value for the control (0.1% v/v DMSO) corresponds to 1, represented in the graph as a dotted line (**$p \leq 0.01$, ***$p \leq 0.001$, ****$p \leq 0.0001$).

These results point out that both complexes are able to increase the intracellular levels of ROS, leading to the induction of apoptosis and autophagy and the loss of cell viability observed at 72 h (Table 3 and Figures 6 and 7). Indeed, other Ru(II) complexes and natural compounds have been described to increase intracellular ROS, triggering apoptosis and autophagy.[72]

Cell Cycle Progression. For further investigation of the cytostatic potential of the complexes in MCF7 tumor cells, cells were previously synchronized at the G1/S phase of the cell cycle and the cell cycle progression of untreated and complex-treated MCF7 cells (for 6, 9, 12, and 24 h) was evaluated by flow cytometry using propidium iodide (PI) labeling. Flow cytometry analysis showed that both complexes do not influence cell cycle progression, since no arrest or delay is observed in comparison to control cells (see Figure S11 in the Supporting Information).

Despite the partial intercalation to DNA observed *in vitro* for both complexes (Figure 4), cell cycle results indicate that DNA might not be a target of the complexes. Considering these results, we might envision other cellular targets such as proteins.

Transport in the Blood Plasma: Interaction with Human Serum Albumin. Plasma proteins are the most prominent metal ion and metal complex binders within all blood components.[30,33] Human serum albumin (HSA) stands out as the major nonspecific transport vehicle in the human blood plasma, accounting for ∼60% of total plasma protein content.[31,73]

Binding of complexes **1** and **2** to human serum albumin was addressed by steady-state fluorescence spectroscopy, using the intrinsic emission of the protein from Trp214, the single tryptophan residue. Trp214 can be selectively excited at 295 nm, and the corresponding emission can be observed at 330−380 nm. Trp214 is located in subdomain IIA within the Sudlow binding site I and is very sensitive to its environment, being able to sense changes occurring in the Sudlow drug binding site II as well.[45,73]

Emission spectra of the protein in the absence and in the presence of increasing concentrations of either complex is depicted in Figure 9A,B. In the case of both complexes, the data follow a linear Stern−Volmer fit in the low protein to complex ratio range, while for higher protein -Ru complex ratios the experimental data are better described by a quadratic fit. These results suggest that two binding events take place in the interaction of these complexes with the protein, one more relevant at low complex concentrations (more pertinent biologically) and another that becomes important at high ratios.

It is possible to estimate conditional binding constants to these binding events in 2% DMSO/Hepes buffer (pH 7). For complex **1**, K_1 and K_2 can be estimated from the quadratic Stern−Volmer fit to data in the low protein to complex ratios (Figure 9C)

$$\frac{I_{F0}}{I_F} = 1 + (1.0497 \times 10^5)C_{complex} + (9.8996 \times 10^8)C_{complex}^2$$

(R^2 = 0.9904), yielding log K_1 = 4.98 and log K_2 = 4.02.

Although the whole set of data can be fit to

https://dx.doi.org/10.1021/acs.inorgchem.0c02768
Inorg. Chem. 2021, 60, 2914−2930

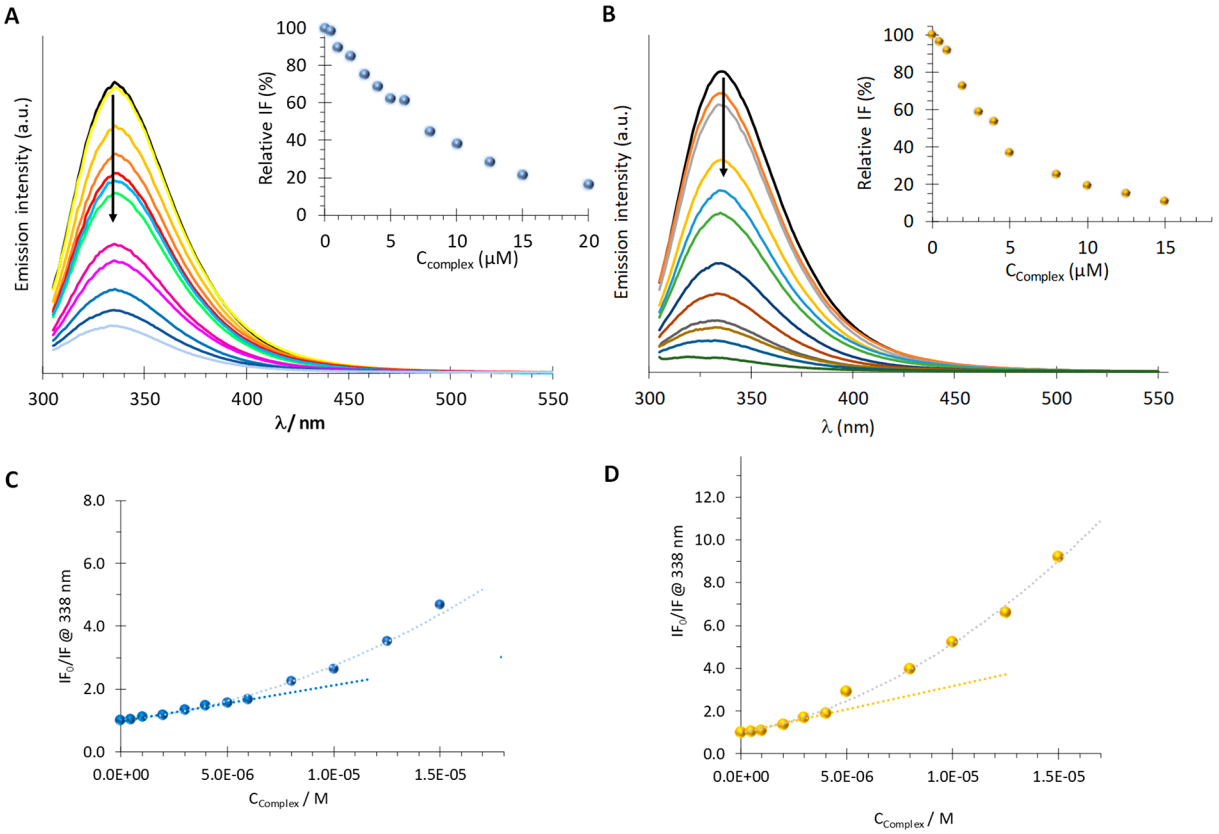

Figure 9. Interaction of Ru complexes with human albumin: HSA-Trp214 emission fluorescence spectrum (λ_{exc} 295 nm) in the presence of complex **1** (A) and complex **2** (B) (black line, HSA alone; colored lines, samples with increasing concentration of complex; emission intensity evolves with increasing concentration as indicated by the arrow; all spectra corrected for inner filter effects); Insets (A and B): change in the relative emission intensity at λ_{em} 338 nm for each complex. Stern−Volmer plots for the quenching of Trp214 emission at 338 nm for the interaction of compounds **1** (C) and **2** (D) with HSA (C_{HSA} = 2 μM; 2% DMSO/Hepes buffer pH 7; 18 h incubation at 37.0 ± 0.5 °C; measurements at room temperature, 23 ± 1 °C; corresponding fits to the experimental data included, see text for details).

$$\frac{I_{F0}}{I_F} = 1 + (4.356 \times 10^4)C_{complex} + (1.309 \times 10^{10})C_{complex}^2$$

(R^2 = 0.9964, all points included), the extraction of physically meaningful values for K_1 and K_2 from this fit is not feasible in a direct manner. However, K_1 can also be estimated from the slope of the Stern−Volmer fit to data at the low protein to complex ratios

$$\frac{I_{F0}}{I_F} = (0.97 \pm 0.04) + (11.5 \pm 1.2) \times 10^4 C_{complex}$$

(R^2 = 0.9921, 95% confidence level) and used to estimate K_2 from the quadratic fit to all experimental points (above, with R^2 = 0.9964). When all of the calculations are taken together, binding constants for the interaction of **1** with HSA are estimated as log K_1 = 5.02 ± 0.06 and log K_2 = 4.8 ± 0.7.

In the case of complex **2**, K_1 was estimated from the Stern−Volmer fit to data at the low protein to complex ratios

$$\frac{I_{F0}}{I_F} = (0.96 \pm 0.1) + (23.0 \pm 4.9) \times 10^4 C_{complex}$$

(R^2 = 0.9867, 95% confidence level) and K_2 was then obtained from the quadratic fit

$$\frac{I_{F0}}{I_F} = 1 + (1.7461 \times 10^5)C_{complex} + (2.4040 \times 10^{10})C_{complex}^2$$

(R^2 = 0.99469, Figure 9D). Binding constants for the interaction of **2** with HSA are thus estimated as log K_1 = 5.36 ± 0.09 and log K_2 = 5.0 ± 0.1.

In conclusion, the remarkable extent of quenching of the HSA-Trp214 emission in the presence of **1** and **2** indicates for both compounds that they are likely to bind HSA close to the Trp214 residue, located in the protein in its domain IIA, and the conditional binding constants estimated show a moderate to strong interaction with human albumin. These results indicate that both complexes might be transported in the blood via albumin binding, allowing for their distribution to tumor sites *in vivo*, possibly with an increased circulation time (that could also act as a drug delivery platform).[74]

Fish Embryo Acute Toxicity Test (FET). Zebrafish embryos and larvae are excellent models for testing *in vivo* the toxicity of complexes.[75] In this sense, we performed a modified FET[39] to evaluate the toxicity of complexes **1** and **2**. For such an analysis, zebrafish embryos were exposed to different concentrations of the tested complexes, as well as positive and negative controls from the early blastula stage. End points were recorded every 24 h up to 96 h postfertilization (hpf).

https://dx.doi.org/10.1021/acs.inorgchem.0c02768
Inorg. Chem. 2021, 60, 2914−2930

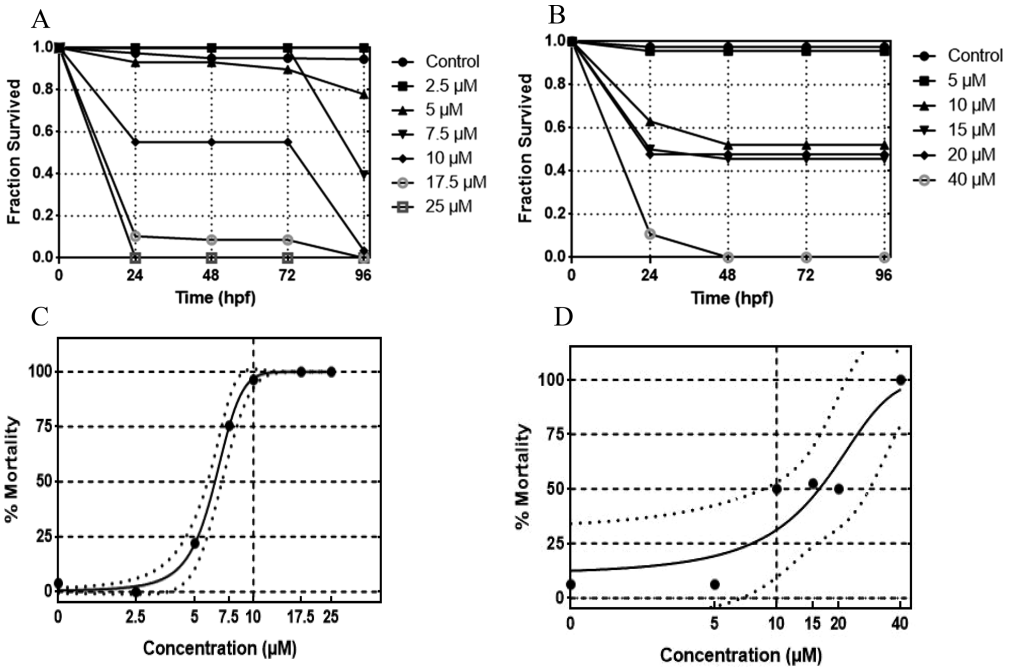

Figure 10. Cumulative toxicity: graphs show fraction of zebrafish without acute toxicity for the tested complexes **1** (A) and **2** (B) at the different stages evaluated (in hpf). Mortality-response curve for tested complexes **1** (C) and **2** (D).

Figure 10 shows the cumulative toxicity for both complexes: that is, the fraction of embryos and larvae with no signs of acute toxicity for the different solutions tested at the evaluated time points. Thus, survival in these graphs refers to the absence of end points. We observed that survival was higher than 90% for negative and solvent controls in all experiments (Figure 10). Although they are not represented in the graphs, embryos were highly sensitive to the positive control, showing >30% mortality. An analysis of the cumulative toxicity for compound **2** shows that it produces acute toxicity mainly within the first 48 h of development, with "coagulated embryo" being the most common end point recorded. For this compound, survival was 50% at 10−20 μM but no survival at 40 μM by 48 h postfertilization (hpf). After this stage, the survival remains quite constant until the end of the test. For compound **1**, signs of acute toxicity appear at two stages of development: within the first 24 h of development and from 72 to 96 hpf. By 24 hpf, the survival is below 50% for the concentrations 17.5 and 25 μM, again "coagulated embryo" being the main end point observed. After this stage, survival remains quite constant but severely decreases from 72 to 96 hpf for concentrations tested above 7.5 μM. This decrease coincides with the period of embryo hatching from the chorion for control and exposed embryos. Thus, as the chorion has barrier properties,[76] an increase in toxicity in this period could be related to the loss of embryo protection by the chorion after hatching.

Figure 10 C,D represents the mortality-response curves for the complexes tested. The response curve for compound **2** shows a smaller slope than for **1**. Confidence interval limits are higher for compound **2** because two replicates showed differences in mortality to the other two for concentrations of 15−20 μM.

On the basis of the results obtained by 96 hpf, we calculated lethal concentration values at which 50% of the embryos show acute toxicity (LC_{50}). For this purpose, data were normalized to the negative and solvent controls and LC_{50} values were calculated for both complexes (Table 4), giving values of 6.33 ± 0.25 μM for complex **1** and 16.06 ± 3.52 μM for complex **2**. Thus, complex **2** is less toxic than complex **1**, with its LC_{50} being more than double.

Table 4. Lethal Concentration Values (LC_{50} (μM)) of Zebrafish Embryos Subjected to Tested Compounds from Early Blastula Stage up to 96hpf Calculated by Logit and Probit Analyses[a]

	LC_{50} at 96 hpf (μM)		
	LC_{50}	CL (95%)	SEM
1	6.33	5.81−6.84	0.25
2	16.06	8.57−23.54	3.52

[a]Definitions: CL, confidence limit; SEM, standard error of the mean.

CONCLUSIONS

Two novel ruthenium(II) complexes derived from η^6-*p*-cymene with a "piano-stool" structure and diphosphane ligands were obtained via substitution reactions and were fully characterized. The general electrochemical behavior of the complexes was characterized by the presence of quasi-reversible or irreversible ruthenium-centered processes at positive potentials (1.67−1.75 V) and ligand-based reductive processes. The high potentials found for the Ru(II)/Ru(III) couple, in particular for complex **1** (E_{pa} = 1.75 V), indicate that the ligand coordination sphere around the metal is suitable to stabilize Ru in the +2 state.

Complexes **1** and **2** are very active against human adenocarcinoma cells of different origins and aggressivenesses: namely, ovary and breast cells including the triple negative breast cancer model. On consideration of the IC_{50} values determined, the activity of these complexes against the adenocarcinoma cells tested followed the trend **1** ≫ **2** and their cytotoxicity seemed to be favored for the breast MCF7 cells. Interestingly, at the IC_{50} values in the MCF7 cancer cells,

https://dx.doi.org/10.1021/acs.inorgchem.0c02768
Inorg. Chem. 2021, 60, 2914−2930

complexes **1** and **2** presented lower cytotoxicity against the normal human primary fibroblasts. Complex **1** in particular showed an intrinsic selectivity for tumor cells with SI values ranging from ∼20 to ∼40 (toward MCF7 cells). Although a direct comparison between literature values must be cautious due to different experimental conditions, IC_{50} values found for complex **1** are (to the best of our knowledge) within the lowest determined for Ru(*p*-cymene) derivatives.

Complexes **1** and **2** enter MCF7 cells via passive diffusion. Complex **1** induced cell detachment, leading to a lower intracellular percent of Ru in adherent cells. Partial intercalation between both complexes and DNA was observed *in vitro*. However, both complexes showed low competitive effects, suggesting that DNA is not a target, a hypothesis that is supported by the fact that no cell cycle delay or arrest was observed in MCF7 cells. The antiproliferative effect of complexes **1** and **2** might be associated with the induction of ROS, which triggered a combined mechanism of apoptosis and autophagy.

Both complexes bind human albumin with moderate to strong affinity, which can be used as a drug delivery platform, allowing the complexes to be transported to the tumor site and increasing their distribution time and efficacy. These results are very interesting for further *in vivo* studies.

In vivo toxicity analysis in zebrafish showed that complex **1** is more toxic than complex **2**. These results are in line with cytotoxicity results, with complex **1** being more active. Nevertheless, this LC_{50} value determined for **1** is ca. 1 order of magnitude higher than any IC_{50} value obtained for all of the tumor cell lines investigated (IC_{50}(**1**) < 0.5 uM).

Overall, the results reported herein support that these complexes seem to have promising therapeutic potential, especially complex **1**, surely justifying further *in vivo* studies in mice.

■ ASSOCIATED CONTENT

Supporting Information

The Supporting Information is available free of charge at https://pubs.acs.org/doi/10.1021/acs.inorgchem.0c02768.

Characterization of complexes ($^{31}P\{^1H\}$ and ^1H NMR spectra, UV−vis spectra, cyclic voltammetry data), stability in solution, cytotoxicity in tumor and normal cells, cell cycle progression (PDF)

Accession Codes

CCDC 1529756−1529757 contain the supplementary crystallographic data for this paper. These data can be obtained free of charge via www.ccdc.cam.ac.uk/data_request/cif, or by emailing data_request@ccdc.cam.ac.uk, or by contacting The Cambridge Crystallographic Data Centre, 12 Union Road, Cambridge CB2 1EZ, UK; fax: +44 1223 336033.

■ AUTHOR INFORMATION

Corresponding Authors

Ana Isabel Tomaz − *Centro de Química Estrutural and Departamento de Química e Bioquímica, Faculdade de Ciências, Universidade de Lisboa, 1049-016 Lisboa, Portugal;* orcid.org/0000-0002-2249-4684; Email: isabel.tomaz@ciencias.ulisboa.pt

Alexandra R. Fernandes − *UCIBIO, Departamento Ciências da Vida, Faculdade de Ciências e Tecnologia, Universidade Nova de Lisboa, 2829-516 Caparica, Portugal;* orcid.org/0000-0003-2054-4438; Email: ma.fernandes@fct.unl.pt

Jesús J. Fernández − *Departamento de Química & Centro de Investigaciones Científicas Avanzadas (CICA), Universidade da Coruña, 15008 A Coruña, Spain;* orcid.org/0000-0003-4938-0342; Email: lujjfs@udc.es

Authors

Oscar A. Lenis-Rojas − *Instituto de Tecnologia Química e Biológica António Xavier, ITQB, 2780-157 Oeiras, Portugal*

M. Paula Robalo − *Área Departamental de Engenharia Química, ISEL-Instituto Superior de Engenharia de Lisboa, Instituto Politécnico de Lisboa, 1959-007 Lisboa, Portugal; Centro de Química Estrutural, Instituto Superior Técnico, Universidade de Lisboa, 1049-001 Lisboa, Portugal*

Catarina Roma-Rodrigues − *UCIBIO, Departamento Ciências da Vida, Faculdade de Ciências e Tecnologia, Universidade Nova de Lisboa, 2829-516 Caparica, Portugal*

Ricardo G. Teixeira − *Centro de Química Estrutural and Departamento de Química e Bioquímica, Faculdade de Ciências, Universidade de Lisboa, 1049-016 Lisboa, Portugal*

Fernanda Marques − *Centro de Ciências e Tecnologías Nucleares (C2TN), Instituto Superior Técnico, Universidade de Lisboa, 2695-066 Bobadela LRS, Portugal*

Mónica Folgueira − *Neurover Group, Centro de Investigacións Científicas Avanzadas (CICA) and Department of Biology, Universidade da Coruña, 15008 A Coruña, Spain; Department of Cell and Developmental Biology, University College London, London WC1 6BT, U.K.*

Julián Yáñez − *Neurover Group, Centro de Investigacións Científicas Avanzadas (CICA) and Department of Biology, Universidade da Coruña, 15008 A Coruña, Spain*

Anabel Alba Gonzalez − *Neurover Group, Centro de Investigacións Científicas Avanzadas (CICA) and Department of Biology, Universidade da Coruña, 15008 A Coruña, Spain*

Martín Salamini-Montemurri − *Neurover Group, Centro de Investigacións Científicas Avanzadas (CICA) and Department of Biology, Universidade da Coruña, 15008 A Coruña, Spain*

Dawrin Pech-Puch − *Departamento de Química & Centro de Investigaciones Científicas Avanzadas (CICA), Universidade da Coruña, 15008 A Coruña, Spain; Departamento de Biología Marina, Universidad Autónoma de Yucatán, C.P. 97100 Mérida, Yucatán, Mexico*

Digna Vázquez-García − *Departamento de Química & Centro de Investigaciones Científicas Avanzadas (CICA), Universidade da Coruña, 15008 A Coruña, Spain*

Margarita López Torres − *Departamento de Química & Centro de Investigaciones Científicas Avanzadas (CICA), Universidade da Coruña, 15008 A Coruña, Spain*

Alberto Fernández − *Departamento de Química & Centro de Investigaciones Científicas Avanzadas (CICA), Universidade da Coruña, 15008 A Coruña, Spain;* orcid.org/0000-0003-2504-6016

Complete contact information is available at: https://pubs.acs.org/10.1021/acs.inorgchem.0c02768

Author Contributions

The manuscript was written through contributions of all authors. All authors have given approval to the final version of the manuscript.

Notes

The authors declare no competing financial interest.

https://dx.doi.org/10.1021/acs.inorgchem.0c02768
Inorg. Chem. 2021, 60, 2914−2930

■ ACKNOWLEDGMENTS

UDC authors acknowledge the financial support received from the Xunta de Galicia (Galicia, Spain) under the Grupos de Referencia Competitiva Programme: Project ED431C 2018/39 (Quimolmat Group). Portuguese authors acknowledge the Portuguese Foundation for Science and Technology (FCT - Fundação para a Ciência e a Tecnologia) for funding through projects PEst 2015-2020, UID/Multi/04349/2013, RECI/QEQ-QIN/0189/2012, and UIDB/QUI/00100/2020. This work was supported by the Applied Molecular Biosciences Unit - UCIBIO that is financed by national funds from the FCT/MCTES (UID/Multi/04378/2020). A.I.T. acknowledges the FCT, POPH-Programa Operacional Potencial Humano, and FSE-European Social Fund for the IF2013-Initiative and for project IF/01179/2013, as well as COST Action NECTAR (CA18202, European Cooperation in Science and Technology). R.G.T. thanks the FCT for his Ph.D. Grant (SFRH/BD/135830/2018). O.A.L.-R. acknowledges Project LISBOA-01-0145-FEDER-007660 (Microbiologia Molecular, Estrutural e Celular) funded by FEDER funds through COMPETE2020-Programa Operacional Competitividade e Internacionalização (POCI) and by national funds through FCT, POPH-*Programa Operacional Potencial Humano*, and FSE (European Social Fund) for the CEEC 2017 Initiative. A. Carvalho is also acknowledged for her contribution to the biological data. A.A.-G. acknowledges the Xunta de Galicia (Galicia, Spain) for funding through a predoctoral fellowship. M.S.-M. acknowledges the Ministry of Science, Innovation and University of Spain for funding through a FPU fellowship. D.P.-P. received a postdoctoral fellowship from the National Council of Science and Technology (CONACYT) of Mexico.

■ ABBREVIATIONS

MS-FAB, fast atom bombardment mass spectroscopy; RP-HPLC, reversed phase high performance liquid chromatography; Λ_m, Specific molar conductivity; ν_s, symmetric stretching vibration mode; ν_{as}, asymmetric stretching vibration mode; CT-DNA, calf thymus DNA; Tris, 2-amino-2-(hydroxymethyl)propane-1,3-diol; Hepes, 4-(2-hydroxyethyl)-1-piperazineethanesulfonic acid; MTT, methyl thiazolyl tetrazolium salt; H_2DCF-DA, 2′,7′-dichlorodihydrofluorescein diacetate; HSA, human serum albumin; ICP-AES, inductively coupled plasma-atomic emission spectrometry; Hepes, 4-(2-hydroxyethyl)-1-piperazineethanesulfonic acid; SDTW, sterile dechlorinated tap water; hpf, hours postfertilization; Hoechst 33258, 2′-[4-ethoxyphenyl]-5-[4-methyl-1-piperazinyl]-2,5′-bi-1*H*-benzimidazole trihydrochloride trihydrate; FET, fish embryo acute toxicology test

■ REFERENCES

(1) (a) Brabec, V.; Kasparsova, J. Modifications of DNA by platinum complexes. Relation to resistance of tumors to platinum antitumor drugs. *Drug Resist. Updates* **2005**, *8*, 131−146. (b) Jung, Y.; Lippard, S. J. Direct Cellular Responses to Platinum-lnduced DNA Damage. *Chem. Rev.* **2007**, *107*, 1387−1407. (c) Bruijnincx, P. C. A.; Sadler, P. J. Controlling Platinum, Ruthenium and Osmium Reactivity for Anticancer Drug Design. *Adv. Inorg. Chem.* **2009**, *61*, 1−62. (d) Brock, P. R.; Knight, K. R.; Freyer, D. R.; Campbell, K. C. M.; Steyger, P. S.; Blakley, B. W.; Rassekh, S. R.; Chang, K. W.; Fligor, B. J.; Rajput, K.; Sullivan, M.; Neuwelt, E. A. Platinum-induced ototoxicity in children: a consensus review on mechanisms, predisposition, and protection, including a new lnternational Society of Pediatric Oncology Boston ototoxicity scale. *J. Clin. Oncol.* **2012**, *30*, 2408−2417. (e) Avan, A.; Postma, T. J.; Ceresa, C.; Avan, A.; Cavaletti, G.; Giovannetti, E.; Peters, G. J. Platinum-lnduced Neurotoxicity and Preventive Strategies: Past, Present, and Future. *Oncologist* **2015**, *20*, 411−432.

(2) Mjos, K. D.; Orvig, C. Metallodrugs in Medicinal Inorganic Chemistry. *Chem. Rev.* **2014**, *114* (8), 4540−4563.

(3) (a) Clarke, M. J. Ruthenium metallopharmaceuticals. *Coord. Chem. Rev.* **2002**, *232*, 69−93. (b) Brabec, V.; Nováková, O. DNA binding mode of ruthenium complexes and relationship to tumor cell toxicity. *Drug Resist. Updates* **2006**, *9*, 111−122. (c) Meng, X.; Leyva, M. L.; Jenny, M.; Gross, I.; Benosman, S.; Fricker, B.; Harlepp, S.; Hébraud, P.; Boas, A.; Wlosik, P.; Bischoff, P.; Sirlin, C.; Pfeffer, M.; Loeffler, J.-P.; Gaiddon, C. A Ruthenium-Containing Organometallic Compound Reduces Tumor Growth through lnduction of the Endoplasmic Reticulum Stress Gene CHOP. *Cancer Res.* **2009**, *69*, 5458−5466. (d) Zeng, L.; Gupta, P.; Chen, Y.; Wang, E.; Ji, L.; Chao, H.; Chen, Z.-S. The development of anticancer ruthenium(II) complexes: from single molecule compounds to nanomaterials. *Chem. Soc. Rev.* **2017**, *46*, 5771−5804.

(4) Bytzek, A. K.; Koellensperger, G.; Keppler, B. K.; Hartinger, C. G. Biodistribution of the Novel Anticancer Drug Sodium Trans-[Tetrachloridobis(1H-Indazole)Ruthenate(III)] KP-1339/IT139 in Nude BALB/c Mice and Implications on Its Mode of Action. *J. Inorg. Biochem.* **2016**, *160* (III), 250−255.

(5) Trondl, R.; Heffeter, P.; Kowol, C. R.; Jakupec, M. A.; Berger, W.; Keppler, B. K. NKP-1339, the first ruthenium-based anticancer drug on the edge to clinical application. *Chem. Sci.* **2014**, *5*, 2925−2932.

(6) Monro, S.; Colón, K. L.; Yin, H.; Roque, J.; Konda, P.; Gujar, S.; Thummel, R. P.; Lilge, L.; Cameron, C. G.; McFarland, S. A. Transition Metal Complexes and Photodynamic Therapy from a Tumor-Centered Approach: Challenges, Opportunities, and Highlights from the Development of TLD1433. *Chem. Rev.* **2019**, *119*, 797−828.

(7) Poynton, F. E.; Bright, S. A.; Blasco, S.; Williams, D. C.; Kelly, J. M.; Gunnlaugsson, T. The development of ruthenium(II) polypyridyl complexes and conjugates for *in vitro* cellular and in vivo applications. *Chem. Soc. Rev.* **2017**, *46* (24), 7706−7756.

(8) (a) Du, Y.; Fu, X.; Li, H.; Chen, B.; Guo, Y.; Zhang, H.; Ning, F.; Lin, Y.; Mei, W.; Chen, T. Mitochondrial fragmentation is an important cellular event induced by ruthenium(II) polypyridyl complexes in osteosarcoma cells. *ChemMedChem* **2014**, *9*, 714−718. (b) Gill, M. R.; Thomas, J. A. Ruthenium(II) polypyridyl complexes and DNA-from structural probes to cellular imaging and therapeutics. *Chem. Soc. Rev.* **2012**, *41*, 3179−3192. (c) Knoll, J. D.; Turro, C. Control and utilization of ruthenium and rhodium metal complex excited states for photoactivated cancer therapy. *Coord. Chem. Rev.* **2015**, *282*−*283*, 110−126. (d) Richter, S.; Singh, S.; Draca, D.; Kate, A.; Kumbhar, A.; Kumbhar, A. S.; Maksimovic-Lvanic, D.; Mijatovic, S.; Liinnecke, P.; Hey-Hawkins, E. Antiproliferative activity of ruthenium(II) arene complexes with mono-and bidentate pyridine-based ligands. *Dalton Trans.* **2016**, *45*, 13114−13125.

(9) Lenis-Rojas, O. A.; Fernandes, A. R.; Roma-Rodrigues, C.; Baptista, P. V.; Marques, F.; Pérez-Fernández, D.; Guerra-Varela, J.; Sánchez, L.; Vázquez-Garcia, D.; López Torres, M.; Fernández, A.; Femández, J. J. Heteroleptic mononuclear compounds of ruthenium-(II): synthesis, structural analyses, in vitro antitumor activity and in vivo toxicity on zebrafish embryos. *Dalton Trans.* **2016**, *45*, 19127−19140.

(10) (a) Riedl, C. A.; Flocke, L. S.; Hejl, M.; Roller, A.; Klose, M. H. M.; Jakupec, M. A.; Kandioller, W.; Keppler, B. K. lntroducing the 4-Phenyl-1,2,3-Triazole Moiety as a Versatile Scaffold for the Development of Cytotoxic Ruthenium(II) and Osmium(II) Arene Cyclometalates. *Inorg. Chem.* **2017**, *56*, 528−541. (b) Dutta, B.; Scolaro, C.; Scopelliti, R.; Dyson, P. J.; Severin, K. lmportance of the, -Ligand: Remarkable Effect of the Cyclopentadienyl Ring on the Cytotoxicity of Ruthenium PTA Compounds. *Organometallics* **2008**, *27*, 1355−1357. (c) Fernández, M.; Rodríguez Arce, E.; Sarniguet, C.; Morais,

https://dx.doi.org/10.1021/acs.inorgchem.0c02768
Inorg. Chem. 2021, 60, 2914−2930

T. S.; Tomaz, A. I.; Olea Azar, C.; Figueroa, R.; Maya, J. D.; Medeiros, A.; Comini, M.; García, M. H.; Otero, L.; Gambino, D. Novel ruthenium(II) cyclopentadienyl thiosemicarbazone compounds with antiproliferative activity on pathogenic trypanosomatid parasites. *J. Inorg. Biochem.* **2015**, *153*, 306−314. (d) Parveen, S.; Arjmand, F.; Tabassum, S. Development and future prospects of selective organometallic compounds as anticancer drug candidates exhibiting novel modes of action. *Eur. J. Med. Chem.* **2019**, *175*, 269−286.

(11) Moreno, V.; Font-Bardia, M.; Calvet, T.; Lorenzo, J.; Avilés, F. X.; García, M. H.; Morais, T. S.; Valente, A.; Robalo, M. P. DNA interaction and cytotoxicity studies of new ruthenium(II) cyclopentadienyl derivative complexes containing heteroaromatic ligands. *J. Inorg. Biochem.* **2011**, *105*, 241−249.

(12) Singh, A. K.; Pandey, D. S.; Xu, Q.; Braunstein, P. Recent advances in supramolecular and biological aspects of arene ruthenium(II) complexes. *Coord. Chem. Rev.* **2014**, *270*−*271*, 31−56.

(13) (a) Murray, B. S.; Babak, M. V.; Hartinger, C. G.; Dyson, P. J. The development of RAPTA compounds for the treatment of tumors. *Coord. Chem. Rev.* **2016**, *306*, 86−114. (b) Sandland, J.; Savoie, H.; Boyle, R. W.; Murray, B. S. Synthesis and In Vitro Biological Evaluation of a Second-Generation Multimodal Water-Soluble Porphyrin-RAPTA Conjugate for the Dual-Therapy of Cancers. *Inorg. Chem.* **2020**, *59*, 7884−7893.

(14) (a) Habtemariam, A.; Melchart, M.; Fernández, R.; Parsons, S.; Oswald, I.; Parkin, A.; Fabbiani, F.; Davidson, J.; Dawson, A.; Aird, R.; Jodrell, D.; Sadler, P. Structure-Activity Relationships for Cytotoxic Ruthenium(II) Arene Complexes Containing N,N-, N,O-, and O,O-Chelating ligands. *J. Med. Chem.* **2006**, *49*, 6858−6868. (b) Schuecker, R.; John, R. O.; Jakupec, M. A.; Arion, V. B.; Keppler, B. K. Water-Soluble Mixed-ligand Ruthenium(II) and Osmium(II) Arene Complexes with High Antiproliferative Activity. *Organometallics* **2008**, *27*, 6587−6595.

(15) Peacock, A. F. A.; Sadler, P. J. Medicinal Organometallic Chemistry: Designing Metal Arene Complexes as Anticancer Agents. *Chem. - Asian J.* **2008**, *3*, 1890−1899.

(16) Sarkar, A.; Acharya, S.; Khushvant, K.; Purkait, K.; Mukherjee, A. Cytotoxic RuII-*p*-cymene complexes of an anthraimidazoledione: halide dependent solution stability, reactivity and resistance to hypoxia deactivation. *Dalton Trans.* **2019**, *48*, 7187−7197.

(17) Süss-Fink, G. Arene Ruthenium Complexes as Anticancer Agents. *Dalton Trans.* **2010**, *39* (7), 1673−1688.

(18) Zheng, K.; Wu, Q.; Ding, Y.; Mei, W. Arene ruthenium(II) Complexes: The Promising Chemotherapeutic Agent in Inhibiting the Proliferation, Migration and Invasion. *Mini-Rev. Med. Chem.* **2016**, *16* (10), 796−803.

(19) Su, W.; Tang, Z.; Li, P. Development of Arene Ruthenium Antitumor Complexes. *Mini-Rev. Med. Chem.* **2016**, *16* (10), 787−95.

(20) Bíró, L.; Farkas, E.; Buglyó, P. Complex Formation between $Ru(\eta^6,$-*p*-Cym$)(H_2O)_3]^{2+}$ and (O,O) Donor Ligands with Biological Relevance in Aqueous Solution. *Dalton Trans.* **2010**, *39* (42), 10272−10278.

(21) Ang, W. H.; Daldini, E.; Scolaro, C.; Scopelliti, R.; Juillerat-Jeannerat, L.; Dyson, P. J. Development of Organometallic Ruthenium-Arene Anticancer Drugs That Resist Hydrolysis. *Inorg. Chem.* **2006**, *45* (22), 9006−9013.

(22) Vock, C. A.; Renfrew, A. K.; Scopelliti, R.; Juillerat-Jeanneret, L.; Dyson, P. J. Influence of the Diketonato Ligand on the Cytotoxicities of [Ru((6-*p*-Cymene)-(R_2 acac)(PTA)]+ Complexes (PTA = 1,3,5-Triaza-7-Phosphaadamantane). *Eur. J. Inorg. Chem.* **2008**, *2008*, 1661−1671.

(23) Płotek, M.; Starosta, R.; Komarnicka, U. K.; Skórska-Stania, A.; Kołoczek, P.; Kyzioł, A. Ruthenium(II) Piano Stool Coordination Compounds with Aminomethylphosphanes: Synthesis, Characterisation and Preliminary Biological Study in Vitro. *J. Inorg. Biochem.* **2017**, *170*, 178−187.

(24) Aliende, C.; Pérez-Manrique, M.; Jalón, F. A.; Manzano, B. R.; Rodríguez, A. M.; Cuevas, J. V.; Espino, G.; Martínez, M. Á.; Massaguer, A.; González-Bártulos, M.; de Llorens, R.; Moreno, V. Preparation of New Half Sandwich Ruthenium Arene Complexes with Aminophosphines as Potential Chemotherapeutics. *J. Inorg. Biochem.* **2012**, *117*, 171−188.

(25) Scolaro, C.; Chaplin, A. B.; Hartinger, C. G.; Bergamo, A.; Cocchietto, M.; Keppler, B. K.; Sava, G.; Dyson, P. J. Tuning the Hydrophobicity of Ruthenium(II)-Arene (RAPTA) Drugs to Modify Uptake, Biomolecular Interactions and Efficacy. *Dalt. Trans.* **2007**, *2* (43), 5065−5072.

(26) Sáez, R.; Lorenzo, J.; Prieto, M. J.; Font-Bardia, M.; Calvet, T.; Omeñaca, N.; Vilaseca, M.; Moreno, V. Influence of PPh_3 Moiety in the Anticancer Activity of New Organometallic Ruthenium Complexes. *J. Inorg. Biochem.* **2014**, *136*, 1−12.

(27) Renfrew, A. K.; Egger, A. E.; Scopelliti, R.; Hartinger, C. G.; Dyson, P. J. Synthesis and Characterisation of the Water Soluble Bis-Phosphine Complex $[Ru(\eta^6$-Cymene$)(PPh_2(o\text{-}C_6H_4O)\text{-}\kappa^2$-P,O)-(pta)$]^+$ and an Investigation of Its Cytotoxic Effects. *C. R. Chim.* **2010**, *13* (8−9), 1144−1150.

(28) (a) Filak, L. K.; Kalinowski, D. S.; Bauer, T. J.; Richardson, D. R.; Arion, V. B. Effect of the Piperazine Unit and Metal-Binding Site Position on the Solubility and Anti-Proliferative Activity of Ruthenium(II)- and Osmium(II)- Arene Complexes of Isomeric Indolo[3,2-c]quinoline-Piperazine Hybrids. *Inorg. Chem.* **2014**, *53*, 6934−6943. (b) Martínez-Alonso, M.; Busto, N.; Jalón, F. A.; Manzano, B. R.; Leal, J. M.; Rodríguez, A. M.; García, B.; Espino, G. Derivation of Structure-Activity Relationships from the Anticancer Properties of Ruthenium(II) Arene Complexes with 2-Aryldiazole Ligands. *Inorg. Chem.* **2014**, *53*, 11274−11288. (c) Pastuszko, A.; Majchrzak, K.; Czyz, M.; Kupcewicz, B.; Budzisz, E. The synthesis, lipophilicity and cytotoxic effects of new ruthenium(II) arene complexes with chromone derivatives. *J. Inorg. Biochem.* **2016**, *159*, 133−141.

(29) Fasano, M.; Curry, S.; Terreno, E.; Galliano, M.; Fanali, G.; Narciso, P.; Notari, S.; Ascenzi, P. The extraordinary ligand binding properties of human serum albumin. *IUBMB Life* **2005**, *57*, 787−796.

(30) Costa Pessoa, J.; Tomaz, I. Transport of therapeutic vanadium and ruthenium complexes by blood plasma components. *Curr. Med. Chem.* **2010**, *17*, 3701−3738.

(31) Peters, T. *All About Albumin: Biochemistry, Genetics and Medical Applications*; Academic Press: San Diego, CA, 1996.

(32) Kratz, F. Albumin as a drug carrier: design of prodrugs, drug conjugates and nanoparticles. *J. Controlled Release* **2008**, *132*, 171−183.

(33) Maeda, H. Tumor-Selective Delivery of Macromolecular Drugs via the EPR Effect: Background and Future Prospects. *Bioconjugate Chem.* **2010**, *21*, 797−802.

(34) Greish, K. Enhanced permeability and retention of macromolecular drugs in solid tumors: a royal gate for targeted anticancer nanomedicines. *J. Drug Target.* **2007**, *15*, 457−464.

(35) (a) Lenis-Rojas, O. A.; Roma-Rodrigues, C.; Fernandes, A. R.; Marques, F.; Pérez-Fernández, D.; Guerra-Vareta, J.; Sánchez, L.; Vázquez-García, D.; López Torres, M.; Fernández, A.; Fernández, J. J. Dinuclear $Ru^{II}(bipy)_2$ Derivatives: Structural, Biological, and in Vivo Zebrafish Toxicity Evaluation. *Inorg. Chem.* **2017**, *56*, 7127−7144. (b) Lenis-Rojas, O. A.; Robalo, M. P.; Tomaz, A. I.; Carvalho, A.; Fernandes, A. R.; Marques, F.; Folgueira, M.; Yáñez, J.; Vázquez-García, D.; López Torres, M.; Fernández, A.; Fernández, J. J. RuII(p-cymene) Compounds as Effective and Selective Anticancer Candidates with No Toxicity in Vivo. *Inorg. Chem.* **2018**, *57*, 13150−13166.

(36) (a) Griepenburg, J. C.; Rapp, T. L.; Carroll, P. J.; Eberwine, J.; Dmochowski, I. J. Ruthenium-caged antisense morpholinos for regulating gene expression in zebrafish embryos. *Chem. Sci.* **2015**, *6*, 2342−2346. (b) Ruble, B. K.; Yeldell, S. B.; Dmochowski, I. J. Caged oligonucleotides for studying biological systems. *J. Inorg. Biochem.* **2015**, *150*, 182−188. (c) Golbaghi, G.; Pitard, I.; Lucas, M.; Haghdoost, M. M.; López de los Santos, Y.; Doucet, N.; Patten, S. A.; Sanderson, J. T.; Castonguay, A. Synthesis and biological assessment of a ruthenium(II) cyclopentadienyl complex in breast cancer cells and on the development of zebrafish embryos. *Eur. J. Med. Chem.* **2020**, *188*, 112030.

https://dx.doi.org/10.1021/acs.inorgchem.0c02768
Inorg. Chem. 2021, 60, 2914−2930

(37) (a) Zon, L. I.; Peterson, R. T. In vivo drug discovery in the zebrafish. *Nat. Rev. Drug Discovery* **2005**, *4*, 35−44. (b) MacRae, C. A.; Peterson, R. T. Zebrafish as tools for drug discovery. *Nat. Rev. Drug Discovery* **2015**, *14*, 721−731. (c) Garcia, G. R.; Noyes, P. D.; Tanguay, R. L. Advancements in zebrafish applications for 21st century toxicology. *Pharmacol. Ther.* **2016**, *161*, 11−21.

(38) (a) DIN, German standard methods for the examination of water, waste water and sludge -Subanimal testing (group T)- Part 6: Toxicity to fish. Determination of the Non-acute-Poisonous Effect of Waste Water to Fish Eggs by Dilution Limits (T 6), DIN 38415-6, German Standardization Organization, 2010; ISO, Water Quality - Determination of the Acute Toxicity of Waste Water to Zebrafish Eggs (Danio rerio), ISO 15088:2007, 2007. (b) Lammer, E.; Carr, G. J.; Wendler, K.; Rawlings, J. M.; Belanger, S. E.; Braunbeck, T. Is the fish embryo toxicity test (FET) with the zebrafish (Danio rerio) a potential alternative for the fish acute toxicity test? *Comp. Biochem. Physiol., Part C: Toxicol. Pharmacol.* **2009**, *149*, 196−209. (c) Busquet, F.; Strecker, R.; Rawlings, J. M.; Belanger, S. E.; Braunbeck, T.; Carr, G. J.; Cenijn, P.; Fochtman, P.; Gourmelon, A.; Hübler, N.; Kleensang, A.; Knöbel, M.; Kussatz, C.; Legler, J.; Lillicrap, A.; Martínez-Jerónimo, F.; Polleichtner, C.; Rzodeczko, H.; Salinas, E.; Schneider, K. E.; Scholz, S.; van den Brandhof, E. J.; van der Ven, L. T.; Walter-Rohde, S.; Weigt, S.; Witters, H.; Halder, M. OECD validation study to assess intra- and inter-laboratory reproducibility of the zebrafish embryo toxicity test for acute aquatic toxicity testing. *Regul. Toxicol. Pharmacol.* **2014**, *69*, 496−511.

(39) OECD: Test Guideline 236, Guideline for Testing of Chemicals, *Fish Embryo Acute Toxicity (FET) Test*. OECD: Paris, France, 2013.

(40) Armarego, W. L. F.; Chai, C. L. L. *Purification of Laboratory Chemicals*, 6th ed.; Butterworth-Heinemann: 2009.

(41) Sheldrick, G. M. A short history of SHELX. *Acta Crystallogr., Sect. A: Found. Crystallogr.* **2008**, *64*, 112−122.

(42) Tomaz, A. I.; Jakusch, T.; Morais, T. S.; Marques, F.; de Almeida, R. F. M.; Mendes, F.; Enyedy, E. A.; Santos, I.; Pessoa, J. C.; Kiss, T.; Garcia, M. H. $[RuII(H5\text{-}C_5H_5)(Bipy)(PPh_3)]^+$, a Promising Large Spectrum Antitumor Agent: Cytotoxic Activity and Interaction with Human Serum Albumin. *J. Inorg. Biochem.* **2012**, *117*, 261−269.

(43) Lakowicz, J. R. Quenching of fluorescence. In *Principles of Fluorescence Spectroscopy*, 3rd ed.; Springer: New York, 2006; Chapter 8, pp 278−327.

(44) Niles, A. L.; Moravec, R. A.; Riss, T. L. Update on in vitro cytotoxicity assays for drug development. *Expert Opin. Drug Discovery* **2008**, *3*, 655−669.

(45) Demoro, B.; de Almeida, R. F. M.; Marques, F.; Matos, C. P.; Otero, L.; Costa Pessoa, J.; Santos, I.; Rodríguez, A.; Moreno, V.; Lorenzo, J.; Gambino, D.; Tomaz, A. I. Screening organometallic binudear thiosemicarbazone ruthenium complexes as potential anti-tumour agents: cytotoxic activity and human serum albumin binding mechanism. *Dalton Trans.* **2013**, *42*, 7131−7146.

(46) Silva, T. F. S.; Martins, L.M.D.R.S.; Guedes da Silva, M. F. C.; Fernandes, A. R.; Silva, A.; Borralho, P. M.; Santos, S.; Rodrigues, C. M. P.; Pombeiro, A. J. L. Cobalt complexes bearing scorpionate ligands: synthesis, characterization, cytotoxicity and DNA deavage. *Dalton Trans.* **2012**, *41*, 12888−12897.

(47) Silva, A.; Luís, D.; Santos, S.; Silva, J.; Mendo, A. S.; Coito, L.; Silva, T. F. S.; Guedes da Silva, M. F. C.; Martins, L.M.D.R.S.; Pombeiro, A. J. L.; Borralho, P. M.; Rodrigues, C. M. P.; Cabral, M. G.; Videira, P. A.; Monteiro, C.; Fernandes, A. R. Biological characterization of the antiproliferative potential of Co(ll) and Sn(IV) coordination compounds in human cancer cell lines: a comparative proteomic approach. Drug Metab. *Drug Metab. Drug Interact.* **2013**, *28*, 167−176.

(48) Das, K.; Beyene, B. B.; Datta, A.; Garribba, E.; Roma-Rodrigues, C.; Silva, A.; Fernandes, A. R.; Hung, C.-H. EPR and electrochemical interpretation of bispyrazolylacetate anchored Ni(II) and Mn(II) complexes: cytotoxicity and anti-proliferative activity towards human cancer cell lines. *New J. Chem.* **2018**, *42*, 9126−9139.

(49) Jakusch, T.; Hollender, D.; Enyedy, E. A.; Sanchez-Gonzalez, C.; Montes-Bayon, M.; Sanz-Medel, A.; Costa Pessoa, J.; Tomaz, I.; Kiss, T. Biospeciation of various antidiabetic VIVO compounds in serum. *Dalton Trans.* **2009**, 2428−2437.

(50) Coutinho, A.; Prieto, M. Ribonuclease T1 and alcohol dehydrogenase fluorescence quenching by acrylamide: A laboratory experiment for undergraduate students. *J. Chem. Educ.* **1993**, *70*, 425.

(51) EU. Directive 2010/63/EU of the European parliament and of the council of 22 September 2010 on the protection of animals used for scientific purposes. *Off. J. EU* 2010, *276*, 33−79.

(52) Russell, W. M. S.; Burch, R. L. *The principles of humane experimental technique*; Methuen: London, England, 1959.

(53) Beekhuijzen, M.; de Koning, C.; Flores-Guillén, M. E.; de Vries-Buitenweg, S.; Tobor-Kaplon, M.; van de Waart, B.; Emmen, H. From cutting edge to guideline: A first step in harmonization of the zebrafish embryotoxicity test (ZET) by describing the most optimal test conditions and morphology scoring system. *Reprod. Toxicol.* **2015**, *56*, 64−76.

(54) Geary, W. The use of conductivity measurements in organic solvents for the characterisation of coordination compounds. *Coord. Chem. Rev.* **1971**, *7*, 81−122.

(55) Johnston, D. H.; Shriver, D. F. Vibrational study of the trifluoromethanesulfonate anion: unambiguous assignment of the asymmetric stretching modes. *Inorg. Chem.* **1993**, *32*, 1045−1047.

(56) Khül, O. *Phosphorus-31 NMR spectroscopy*; Springer: Berlin, 2008.

(57) Garrou, P. E. $_R$ contributions to phosphorus-31 NMR parameters of transition-metal-phosphorus chelate complexes. *Chem. Rev.* **1981**, *81*, 229−266.

(58) Lalrempuia, R.; Carroll, P. J.; Kollipara, M. R. Syntheses of $[(\eta^6\text{-}p\text{-cymene})Ru(EPh_3)_2Cl]^+$ complexes and molecular structure of chloro(η^6-*p*-cymene)-bis(triphenylphosphine)ruthenium(II) tetrafluoroborate (E = P, As and Sb). *J. Coord. Chem.* **2003**, *56*, 1499−1504.

(59) (a) de los Ríos, I.; Jiménez Tenorio, M.; Jiménez Tenorio, M. A.; Puerta, M. C.; Valerga, P. Synthesis of Cationic Arene Complexes of Iron and Ruthenium with 1,2-Bis(Diisopropylphosphino)Ethane (Dippe): X-Ray Crystal Structures of $[RuCl(V^6\text{-}C_6H_6)(Dippe)][BPh_4]$ and $[RuH(({}^6\text{-}C_6H_6)(Dippe)][BPh_4]$. *J. Organomet. Chem.* **1996**, *525* (1−2), 57−64. (b) Daguenet, C.; Scopelliti, R.; Dyson, P. J. Mechanistic lnvestigations on the Hydrogenation of Alkenes Using Ruthenium(II)-Arene Diphosphine Complexes. *Organometallics* **2004**, *23*, 4849−4857. (c) Therrien, B.; Suss-Fink, G.; Govindaswamy, P.; Said-Mohamed, C. Mono and di nuclear arene ruthenium complexes containing 6,7-dimethyl-2,3-di(pyridine-2-yl)quinoxaline as chelating ligand: Synthesis and molecular structure. *Polyhedron* **2007**, *26*, 4065−4072.

(60) Štarha, P.; Trávnícek, Z.; Krikavová, R.; Dvorák, Z. Half-Sandwich Ru(II) Halogenido, Valproato and 4-Phenylbutyrato Complexes Containing 2,2′-Dipyridylamine: Synthesis, Characterization, Solution Chemistry and In Vitro Cytotoxicity. *Molecules* **2016**, *21*, 1725.

(61) Anjomshoa, M.; Torkzadeh-Mahani, M. Competitive DNA-Binding Studies between Metal Complexes and GelRed as a New and Safe Fluorescent DNA Dye. *J. Fluoresc.* **2016**, *26*, 1505−1510.

(62) Peixoto, D.; Figueiredo, M.; Malta, G.; Roma-Rodrigues, C.; Baptista, P. V.; Fernandes, A. R.; Barroso, S.; Carvalho, A. L.; Afonso, C. A.; Ferreira, L. M.; Branco, P. S. Synthesis, Cytotoxicity Evaluation in Human Cell Unes and in Vitro DNA lnteraction of Hetero-Arylidene-9(10H)-Anthrone. *Eur. J. Org. Chem.* **2018**, *2018*, 545−549.

(63) Morais, T. S.; Valente, A.; Tomaz, A. I.; Marques, F.; Garcia, M. H. Tracking antitumor metallodrugs: promising agents with the Ru(II)- and Fe(ll)-cyclopentadienyl scaffolds. *Future Med. Chem.* **2016**, *8*, 527−544.

(64) Côrte-Real, L.; Mendes, F.; Coimbra, J.; Morais, T. S.; Tomaz, A. I.; Valente, A.; Garcia, M. H.; Santos, I.; Bicho, M.; Marques, F. Anticancer activity of structurally related ruthenium(II) cyclopentadienyl complexes. *JBIC, J. Biol. Inorg. Chem.* **2014**, *19*, 853−867.

https://dx.doi.org/10.1021/acs.inorgchem.0c02768
Inorg. Chem. 2021, 60, 2914−2930

(65) Côrte-Real, L.; Robalo, M. P.; Marques, F.; Nogueira, G.; Avecilla, F.; Silva, T. J. L.; Santos, F. C.; Tomaz, A. I.; Garcia, M. H.; Valente, A. The key role of coligands in novel ruthenium(ll)-cyclopentadienyl bipyridine derivatives: Ranging from nontestingcytotoxic to highly cytotoxic compounds. *J. Inorg. Biochem.* **2015**, *150*, 148−159.
(66) Moreira, T.; Francisco, R.; Comsa, E.; Duban-Deweer, S.; Labas, V.; Teixeira-Gomes, A. P.; Combes-Soia, L.; Marques, F.; Matos, A.; Favrelle, A.; Rousseau, C.; Zinck, P.; Falson, P.; Garcia, M. H.; Preto, A.; Valente, A. Polymer "ruthenium-cyclopentadienyl"conjugates - New emerging anti-cancer drugs. *Eur. J. Med. Chem.* **2019**, *168*, 373−384.
(67) Chuklin, P.; Chalermpanaphan, V.; Nhukeaw, T.; Saithong, S.; et al. Synthesis, X-ray structure of organometallic ruthenium (II) p-cymene complexes based on P- and N- donor ligands and their in vitro antibacterial and anticancer studies. *J. Organomet. Chem.* **2017**, *846*, 242−250.
(68) Almeida, J.; Roma-Rodrigues, C.; Mahmoud, A. G.; Guedes da Silva, M. F. C.; Pombeiro, A. J. L.; Martins, L.M.D.R.S.; Baptista, P. V.; Fernandes, A. R. Structural characterization and biological properties of silver(I) tris(pyrazolyl)methane sulfonate. *J. Inorg. Biochem.* **2019**, *199*, 110789.
(69) D'Arcy, M. S. Cell Death: A Review of the Major Forms of Apoptosis, Necrosis and Autophagy. *Cell Biol. Int.* **2019**, *43* (6), 582−592.
(70) Fulda, S.; Kögel, D. Cell death by autophagy: emerging molecular mechanisms and implications for cancer therapy. *Oncogene* **2015**, *34*, 5105−5113.
(71) Svahn, N.; Moro, A. J.; Roma-Rodrigues, C.; Puttreddy, R.; Rissanen, K.; Baptista, P. V.; Fernandes, A. R.; Lima, J. C.; Rodríguez, L. The lmportant Role of the Nuclearity, Rigidity, and Solubility of Phosphane Ligands in the Biological Activity of Gold(I) Complexes. *Chem. - Eur. J.* **2018**, *24*, 14654−14667.
(72) (a) Gao, L.; Loveless, J.; Shay, C.; Teng, Y. Targeting ROS-Mediated Crosstalk between Autophagy and Apoptosis in Cancer. *Adv. Exp. Med. Biol.* **2020**, *1260*, 1−12. (b) Zhao, Q.; Liu, Y.; Zhong, J.; Bi, Y.; Liu, Y.; Ren, Z.; Li, X.; Jia, J.; Yu, M.; Yu, X. Pristimerin Induces Apoptosis and Autophagy via Activation of ROS/ASK1/JNK Pathway in Human Breast Cancer in Vitro and in Vivo. *Cell Death Discovery* **2019**, *5* (1), 125. (c) Tan, C.; Lai, S.; Wu, S.; Hu, S.; Zhou, L.; Chen, Y.; Wang, M.; Zhu, Y.; Lian, W.; Peng, W.; Ji, L.; Xu, A. Nuclear Permeable Ruthenium(II) *β*-Carboline Complexes Induce Autophagy to Antagonize Mitochondrial-Mediated Apoptosis. *J. Med. Chem.* **2010**, *53* (21), 7613−7624.
(73) Colmenarejo, G. In silico prediction of drug-binding strengths to human serum albumin. *Med. Res. Rev.* **2003**, *23*, 275−301.
(74) Larsen, M. T.; Kuhlmann, M.; Hvam, M. L.; Howard, K. A. Albumin-Based Drug Delivery: Harnessing Nature to Cure Disease. *Mol. Cell. Ther.* **2016**, *4* (1), 3.
(75) (a) Ali, S.; Champagne, D.; Spaink, H.; Richardson, M. Zebrafish embryos and larvae: A new generation of disease models and drug screens. *Birth Defects Res., Part C* **2011**, *93*, 115−133. (b) Haldi, M.; Harden, M.; D'Amico, L.; DeLise, A.; Seng, W. L. Developmental Toxicity Assessment in Zebrafish. In *Zebrafish: methods for assessing drug safety and toxicity*; Wiley: 2012.
(76) (a) Henn, K.; Braunbeck, T. Dechorionation as a tool to improve the fish embryo toxicity test (FET) with the zebrafish (Danio rerio). *Comp. Biochem. Physiol., Part C: Toxicol. Pharmacol.* **2011**, *153*, 91−98. (b) Kais, B.; Schneider, K. E.; Keiter, S.; Henn, K.; Ackermann, C.; Braunbeck, T. DMSO modifies the permeability of the zebrafish (Danio rerio) chorion-lmplications for the fish embryo test (FET). *Aquat. Toxicol.* **2013**, *140*−*141*, 229−238.

https://dx.doi.org/10.1021/acs.inorgchem.0c02768
Inorg. Chem. 2021, 60, 2914−2930